Advances in Water Resources 51 (2013) 197–216

Contents lists available at SciVerse ScienceDirect

Advances in Water Resources

journal homepage: www.elsevier.com/locate/advwatres

Pore-scale imaging and modelling

Martin J. Blunt [a,*], Branko Bijeljic [a], Hu Dong [b], Oussama Gharbi [a], Stefan Iglauer [c], Peyman Mostaghimi [a], Adriana Paluszny [a], Christopher Pentland [a]

[a] Department of Earth Science and Engineering, Imperial College, London SW7 2AZ, UK
[b] iRock Technologies, Suite 1103, Tower A, Oriental Media Center, No. 4 Guanghua Road, Chaoyang District, Beijing 100026, China
[c] Department of Petroleum Engineering, Curtin University, 6151 Perth, Australia

ARTICLE INFO

Article history:
Available online 3 April 2012

Keywords:
Network modelling
Imaging
Relative permeability
Pore-scale

ABSTRACT

Pore-scale imaging and modelling – digital core analysis – is becoming a routine service in the oil and gas industry, and has potential applications in contaminant transport and carbon dioxide storage. This paper briefly describes the underlying technology, namely imaging of the pore space of rocks from the nanometre scale upwards, coupled with a suite of different numerical techniques for simulating single and multiphase flow and transport through these images. Three example applications are then described, illustrating the range of scientific problems that can be tackled: dispersion in different rock samples that predicts the anomalous transport behaviour characteristic of highly heterogeneous carbonates; imaging of super-critical carbon dioxide in sandstone to demonstrate the possibility of capillary trapping in geological carbon storage; and the computation of relative permeability for mixed-wet carbonates and implications for oilfield waterflood recovery. The paper concludes by discussing limitations and challenges, including finding representative samples, imaging and simulating flow and transport in pore spaces over many orders of magnitude in size, the determination of wettability, and upscaling to the field scale. We conclude that pore-scale modelling is likely to become more widely applied in the oil industry including assessment of unconventional oil and gas resources. It has the potential to transform our understanding of multiphase flow processes, facilitating more efficient oil and gas recovery, effective contaminant removal and safe carbon dioxide storage.

1. Introduction

In the last 10 years, pore-scale modelling has developed rapidly from a technique principally devoted to understanding displacement processes with no commercial exploitation, to a predictive tool used in the oil industry with several new companies now providing digital core analysis services. The foundation of this development is the construction of models of increasing sophistication and predictive power that represent both the multiphase flow dynamics and the geometry of the rock [1–11]. This transformation has also been facilitated by the now-routine use of direct three-dimensional imaging of the pore space [12]. This enables predictions to be made on many images of small rock samples, providing data that would be much more difficult – or impossible – to obtain using traditional experimental methods [10,13].

We will first, briefly, mention the imaging methods that are used to produce three-dimensional representations of the pore space of rocks. This topic is the subject of a more detailed review in this issue [14]. We will then discuss the different numerical approaches that are used to compute pore-space properties. These can be divided into two classes: direct simulation, where the governing equations of flow and transport are computed on the image itself; and network modelling, where first a topologically representative network is extracted from the image through which the relevant displacement and transport equations are computed. The strengths and weaknesses of both approaches are presented.

The paper will focus on three applications of imaging and predictive modelling, of interest to the authors, that cover a range of possible application: dispersion in carbonates to elucidate the signature of anomalous transport in highly heterogeneous media; capillary trapping of super-critical carbon dioxide (CO_2) to show that capillary trapping could be an effective and efficient long-term storage mechanism in aquifers; and the relative permeability of mixed-wet carbonates that has implications for waterflood oil recovery in giant Middle Eastern reservoirs. The work builds on the overview of pore-scale modelling published 10 years ago [1], emphasising new developments, particularly the application of pore-scale imaging and the use of predictive approaches to understand carbonates.

We show exemplar applications that illustrate the potential for pore-scale modelling to improve our understanding of different underground flow processes and to help design effective storage,

* Corresponding author.
E-mail address: m.blunt@imperial.ac.uk (M.J. Blunt).

0309-1708 © 2012 Elsevier Ltd. Open access under CC BY-NC-ND license.
http://dx.doi.org/10.1016/j.advwatres.2012.03.003

clean-up and recovery schemes. This paper is not intended as an exhaustive review of different pore-scale modelling applications. Pore-scale modelling is likely to become a standard and invaluable tool in reservoir management, as well as helping to ensure secure carbon dioxide storage and effective contaminant clean-up. In addition, high-resolution imaging could be used to assess unconventional oil and gas resources. However, not all the problems in this field are solved and the paper will end with an overview of difficulties and challenges: upscaling and representative sampling, the determination of wettability, and use of the results in field-scale simulation.

2. Imaging techniques

2.1. X-rays

The development of modern imaging methods relies on the acquisition of three-dimensional reconstructions from a series of two-dimensional projections taken at different angles: the sample is rotated and the absorption of X-rays in different directions is recorded and used to produce a three-dimensional representation of the rock and fluids. In the 1980s these methods were first applied in laboratory-based systems to measure two and three-phase fluid saturations for soil science [15] and petroleum [16] applications with a resolution of around 1–3 mm. The first micro-CT (micron or pore-scale) images of rocks were obtained by Flannery and co-workers at Exxon Research [17] using both laboratory and synchrotron sources. In a synchrotron a bright monochromatic beam of X-rays is shone through a small rock sample. Several rocks were studied with resolutions down to around 3 μm. Dunsmuir et al. extended this work to characterise pore space topology and transport in sandstones [18–20]. Hazlett was the first to use X-ray images for the direct computation of multiphase flow, including predictions of relative permeability, using the lattice Boltzmann method, which is described later [21]. An excellent overview of these imaging techniques applied to the earth sciences is provided by Ketcham and Carlson [22].

One of the pioneers of the continued development of this technology has been the team at the Australian National University in collaboration with colleagues at the University of New South Wales. They have built a bespoke laboratory facility to image a wide variety of rock samples and then predict flow properties [10,13,23,24]. The base image is a three-dimensional map of X-ray absorption; this is thresholded to elucidate different mineralogies, clays and, principally, to distinguish grain from pore space. We will discuss later the use of similar methods [20] to image multiphase distributions.

The now-standard approach to image the pore space of rocks is to use a laboratory instrument, a micro-CT scanner, that houses its own source of X-rays [10]. Here the X-rays are polychromatic and the beam is not collimated – the image resolution is determined primarily by the proximity of the rock sample to the source. These machines offer the advantage that access to central synchrotron facilities or a custom-designed laboratory is not required, and there is no constraint on the time taken to acquire the image, allowing signal to noise to be improved. The disadvantage is that the intensity of the X-rays is poor compared to synchrotrons while the spreading of the beam and the range of wavelengths introduces imaging artefacts.

Fig. 1 shows two-dimensional cross-sections of three-dimensional grey scale images for eight representative rock samples: several carbonates, including a reservoir sample, a sandstone and a sand pack. Table 1 provides a summary of the rocks analyzed in this paper, their properties and details of the overall image and voxel size. The images were acquired either with a synchrotron beamline (SYRMEP beamline at the ELETTRA synchrotron in Trieste, Italy) or from a micro-CT instrument (Xradia Versa).

The first three images in Fig. 1(a)–(c), are carbonates that will be used in our discussion of network extraction (Section 3) and prediction of multiphase flow properties (Section 6). The second row, Fig. 1(d)–(f), shows samples that will be used in our analysis of dispersion in Section 4. For the quarry carbonates (Estaillades, Ketton, Portland, Guiting and Mount Gambier) a connected pore space is resolved, although the details of the structure are complex and at least two of the samples – Ketton and Guiting – are likely to contain significant micro-porosity that is not captured. Also included is a carbonate from a Middle Eastern aquifer, Fig. 1(g). In this case, while some pores are shown with a voxel size of almost 8 μm, it is likely that there is significant connectivity provided by pores that are below the resolution of the image.

Fig. 2 shows example three-dimensional images of three carbonates where only the pore space is shown; networks (see later) will be extracted from these images for a study of multiphase flow and relative permeability in Section 6. Ketton is a classic oolitic limestone composed of almost spherical grains with large, well-connected pores between them. Estaillades has a much more complex structure with some very fine features that may not be fully captured by the image. Mount Gambier has a very irregular pore space, but it is well connected and the porosity and permeability are very high (Table 1). Overall, while a resolution of a few microns can resolve the pore space for some permeable sandstones and carbonates, many carbonates and unconventional sources, such as shales, contain voids that have typical sizes of much less than a micron. If this fraction of the pore space is ignored, it is possible that the resultant transport predictions are significantly in error.

Typical X-ray energies are in the range 30–160 keV for micro-CT machines – with corresponding wavelengths 0.04–0.01 nm – while synchrotrons have beams of different energies for which those with energies less than around 30 keV are ideal for imaging rock samples. Resolution is determined by the sample size, beam quality and the detector specifications; for cone-beam set-ups (in laboratory-based instruments) resolution is also controlled by the proximity of the sample to the beam, while detecting absorption at a sufficiently fine resolution. Current micro-CT scanners will produce images of around 1000^3–2000^3 voxels. To generate a representative image, the cores are normally a few mm across, constraining resolution to a few microns; sub-micron resolution is possible using specially designed instruments and smaller samples. Developments in synchrotron imaging may allow much larger images to be acquired, but at present most images have an approximately 1000-fold range from resolution to sample size.

In this paper, once the images have been obtained, they are processed and segmented into grain and different fluid phases. The pre-segmentation processing of the images involves two main steps: removing noise and destriping. Noise and ring artefacts may originate during acquisition and must be removed prior to the segmentation phase. Ring artefacts are best removed from the original sinograms, in which they appear as vertical noise stripes, using Fourier–Wavelet filtering [25]. If sinogram images are not available, it is necessary to transform the images to polar coordinates, subsequently remove the vertical stripes, and transform results back to Cartesian coordinates. Salt-and-pepper noise is removed using a two-dimensional, or ideally three-dimensional, anisotropic diffusion filter with a high diffusion limiter along maximal variations for edge preservation [26]. Finally, segmentation is performed based on multi-thresholding based on Otsu's algorithm [27]. In the presence of high density minerals, results are best if the number of segmented domains is increased to capture minerals using a separate threshold [28], and to capture any shadows of contrast-agent dosed media. The quality of the ensuing segmentation will depend on the resolution of the initial data, effective

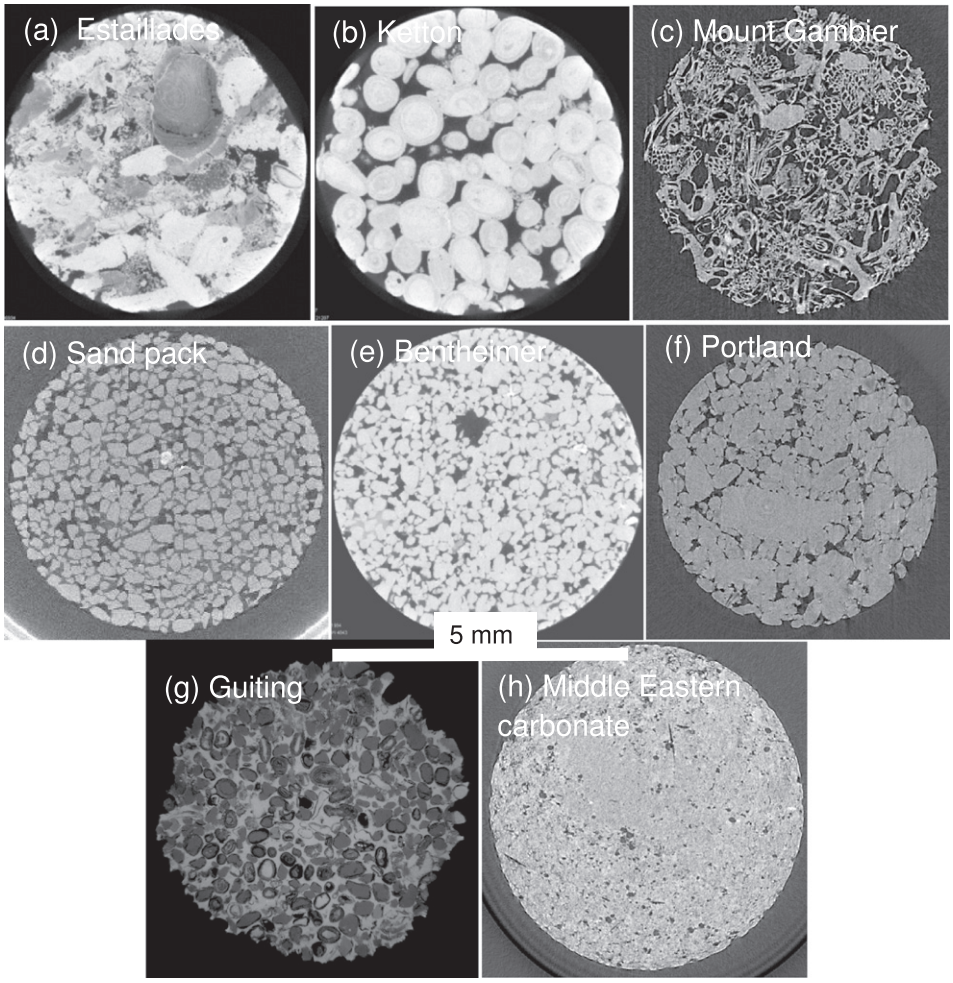

Fig. 1. Two-dimensional cross-sections of three-dimensional micro-CT images of different samples. These are grey scale images where the pore space is shown dark. (a) Estaillades carbonate. The pore space is highly irregular with likely micro-porosity that cannot be resolved. (b) Ketton limestone, an oolitic quarry limestone of Jurassic age. The grains are smooth spheres with large pore spaces. The grains themselves contain micro-pores that are not resolved. (c) Mount Gambier limestone is of Oligocene age from Australia. This is a high-porosity, high-permeability sample with a well-connected pore space. (d) A sand pack of angular grains. (e) Bentheimer sandstone, a quarry stone used in buildings, including the pedestal of the Statue of Liberty in New York. (f) Portland limestone. This is another oolitic limestone of Jurassic age that is well-cemented with some shell fragments. Portland is another building material used, for instance, in the Royal of School of Mines at Imperial College. (g) Guiting carbonate is another Jurassic limestone, but the pore space contains many more shell fragments and evidence of dissolution and precipitation. (h) Carbonate from a deep highly-saline Middle Eastern aquifer.

Table 1
Summary of the rocks and images studied in this paper.

Sample	Figures	Scanner	Image size, voxels	Voxel size, μm	Porosity	Permeability, D^a	Use
Estaillades carbonate	1(a) and 2(a)	Micro-CT	2000^3; 1000^3 For analysis	2.68	0.138*	0.0864*	Relative permeability, Section 6
Ketton limestone	1(b) and 2(b)	Micro-CT	2000^3; 1000^3 For analysis	2.65	0.148*	8.98*	Relative permeability, Section 6
Mount Gambier carbonate	1(c) and 2(c)	Synchrotron	566^3; 350^3 For analysis	9	0.556*	19.2*	Relative permeability, Section 6
Sand pack	1(d) and 4(a)	Micro-CT	600^3; 300^3 For analysis	10	0.372*	39*	Dispersion, Section 4
Bentheimer sandstone	1(e) and 4(b)	Micro-CT	2000^3; 300^3 For analysis	3.0	0.20*	1.4*	Dispersion, Section 4
Portland limestone	1(f) and 4(c)	Synchrotron	601^3; 300^3 For analysis	9	0.092*	0.30*	Dispersion, Section 4
Guiting limestone	1(g)	Micro-CT	2000^3	2.65	0.23*	0.15*	Illustration only
Reservoir carbonate	1(h)	Synchrotron	650^3	7.7	0.15*	0.0327*	Illustration only
Doddington sandstone	7	Micro-CT	600^3	13.7	0.207**	1.6**	Capillary trapping, Section 5

[a] $D = 9.87 \times 10^{-13}$ m^2.
* Computed from the image.
** Measured on larger core samples from the same block of stone.

removal of noise, and on the application of suitable thresholding parameters. Optimal thresholding and noise reduction to delineate multiple phases and to make the best use of raw images is still an area of active research. The segmentation is dependent on the

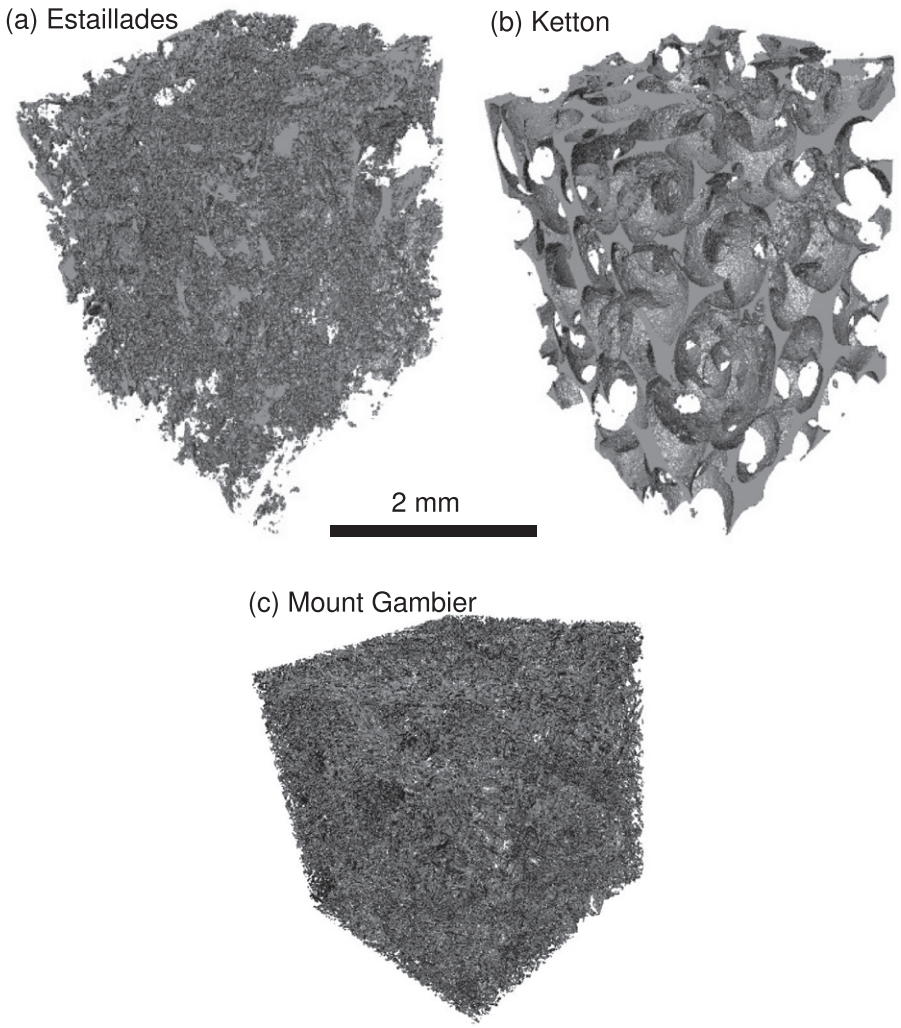

Fig. 2. Pore-space images of three quarry carbonates: (a) Estaillades; (b) Ketton; (c) Mount Gambier. The images shown in cross-section in Figs. 1(a)–(c) have been binarized into pore and grain. A central 1000^3 (Estaillades and Ketton) or 350^3 (Mount Gambier) section has been extracted. The images show only the pore space. Networks will be extracted from these images, Fig. 3, and used in Section 6 for an analysis of multiphase flow and relative permeability.

choice of approach and introduces a major uncertainty in our interpretation of the results. This is discussed in more detail elsewhere [14].

2.2. Focused ion beams

There are other methods, well established in two dimensions, to produce very fine-scale images of rock samples. The most widely applied is SEM – scanning electron microscopy – that routinely produces images down to resolutions of 10s nm. This is sufficient to image the pore spaces in even low permeability sandstones and carbonates and can also study the nm-scale pores in unconventional shale gas and shale oil reserves. The problem is that the images are two-dimensional and hence the three-dimensional connectivity of the pore space is unknown.

FIB/SEM – where FIB stands for focussed ion beams – is a new technology that acquires very high resolution three-dimensional images of tiny rock samples (typically just a few μm across) [29,30]. The ion beam makes very fine slices through the sample, enabling sequential SEM images to be obtained. The method is destructive but reveals unrivalled detail of small pore spaces [29,30].

In addition to SEM and X-rays, light microscopy can be used to produce three-dimensional pore-space images. Confocal microscopy focuses on a series of planes through the sample from which a three-dimensional image is obtained [31]. The vertical resolution can be excellent, but only relatively thin samples can be studied.

Overall, a suite of imaging methods are now available that allow images of rocks to be made at a variety of scales, from the whole core (cm to m to determine heterogeneity and structure) to microns (for the larger pore spaces) and sub-micron for tighter samples.

2.3. Statistical reconstruction

Statistical methods, based on an analysis of a high-resolution two-dimensional image, can be used to construct three-dimensional representations of the pore space. These can be methods that extract typical patterns – essentially multiple-point statistics [32] – to preserve connectivity [33–35] or object-based methods that simulate the packing of irregular grains and subsequent diagenesis [4]. These methods have been extended to allow the representation of the pore space at multiple scales, combining information from images of different resolution and offering a

greater spatial range than any single direct imaging technology alone [35,36].

While brief, this overview serves to highlight that it has been the ability to image pore spaces, or at least generate pore-space representations, that has provided new impetus to pore-scale modelling. The challenge is to take advantage of the information contained in these images: to make reliable and accurate predictions, and to glean new insight into transport behaviour.

3. Modelling methods

There are two ways to compute properties in the pore space. The first is to discretize the voids – usually simply using the Cartesian grid derived from a binarized three-dimensional image – and compute flow and transport on this grid. This is a direct approach and honours – to the limit of the imaging – the geometry of the pore space. The problem is that for the key application of interest, at least for oil recovery – slow flow of multiple phases – most existing techniques are computationally demanding. An alternative methodology is first to extract a topologically representative network with idealised properties derived from the underlying image. Flow and transport are then computed – usually semi-analytically – through this network. This approach is naturally suited for the study of capillary-controlled displacement, while allowing effectively infinite resolution in the network elements. However, it clearly makes a number of approximations concerning the pore space geometry. We discuss both approaches below.

3.1. Direct modelling

The most popular approach for computing single and multiphase flow directly on pore-space images is the lattice Boltzmann method [18,37–44]. This is a particle-based technique that simulates the motion and collision of particles on a grid; the averaged behaviour can be shown to approximate the governing Navier–Stokes equation. The method is relatively easy to code and is ideally suited for parallel computing platforms. It is readily extended to multiphase flow by allowing particles representing fluid elements of two (or more) phases to be tracked. Its main disadvantage is computational efficiency, even with a massively parallel implementation. The run time scales approximately as the inverse of real flow rate, which makes it difficult to capture accurately capillary-controlled displacement on sufficiently large samples to make reliable predictions of relative permeability. However, recent research indicates that with the best computer resources, it is possible to compute relative permeability based on pore-space images in some cases [42–45]. The method is well suited for computing single-phase flow properties and transport, such as permeability, dispersion coefficients and effective reaction rates. It has also been successfully used, for instance, to provide a careful analysis of pore-scale dynamics, to compute interfacial area and to aid the development of improved theories of porous media flow [37–41].

The lattice Boltzmann method is one of a number of particle-based methods, where particles representing packets of fluid are tracked through the computational domain. It is possible to allow these packets to carry averaged properties, such as pressure and density. These effective particles can represent different phases and interact with each other with an equivalent interfacial tension. Smooth particle hydrodynamics and its variants is another method that has been applied successfully to study dispersion and multiphase flow [46,47].

In addition, there are other techniques designed specifically to study capillary-controlled displacement. The level set method defines an interface between fluids and tracks its movement in a quasi-static displacement. This allows complex boundaries to be handled naturally and has no constraint on the topology of the interface. For large problems – based on three-dimensional pore space images – this method is also computationally demanding, but it has been used to offer interesting insights into imbibition processes and fracture/matrix interaction [48,49].

Last, there are conceptually more traditional approaches that solve the Navier–Stokes equation using standard discretization schemes. For slow flow, this can be simplified to the Stokes equation. The computational difficulty rests on tracking and specifying fluid interfaces in multiphase flow. Again there are a variety of methods to achieve this, of which the volume of fluid technique is one of the most promising [50–52]. Here the partial saturation of a phase in a grid block is used to assess the likely location of a sharp interface. The method was originally developed for fluid dynamics applications where capillarity provides a perturbation to a viscous-dominated displacement. The extension to porous media problems, where in general viscous forces are a perturbation to capillary-dominated displacement, is a challenge [52]. Again, as the flow rate decreases, the computational time increases, making direct simulation of capillary-controlled displacement on large pore-space images difficult.

Density functional modelling can also be used to develop a general formulation for fluid flow, incorporating different physical phenomena, including multiphase flow, non-Newtonian rheology and thermal effects [53]. The technique has successfully analyzed fluid distributions in simple geometries representing a single capillary tube but is – like many of these methods – some way from the prediction of core-scale multiphase flow properties based on realistic pore-space images.

This paper will not discuss these methods and results in detail: the reader is invited to read the recent review by Meakin and Tartakovsky [54]. It is likely, with improvements in computer power and numerical methods, that soon most computations of single and multiphase flow properties will be made using one or more of the techniques above, or modifications of them. In particular, methods that embrace new computational platforms, such as massively parallel processing or GPUs (graphical processing units) are likely to flourish. However, at present, while these approaches work well for single-phase flow – for instance we will use a Stokes solver later in this paper to simulate dispersion – they become considerably more cumbersome for multiphase flow, where it is necessary to locate and track interfaces between phases in a complex geometry with contact angles that vary on a pore-by-pore basis. The curvature of this interface controls the capillary pressure that typically dominates over viscous forces. As a consequence, the tracking of these interfaces is exceptionally important. Furthermore, the limited resolution of the computational grid means that it is difficult to resolve thin wetting layers that control many processes in two and three-phase flow [1,7,8]; this limitation is discussed further at the end of the paper. In the literature to date, the most computationally efficient and successful predictions of multiphase flow come from network modelling, described below.

3.2. Network modelling

The first network models were constructed by Fatt, who exploited the analogy between flow in porous media and a random resistor network [55]. Since then the models have grown hugely in sophistication and now can accommodate irregular lattices, wetting layer flow, arbitrary wettability and any sequence of displacement in two- and three-phase flow, as well as a variety of different physical processes, including phase exchange, non-Newtonian displacement, non-Darcy flow, reactive transport and thermodynamically consistent oil layers (see, for instance [1,56–59]). Most of the underlying mechanisms for capillary-dominated immiscible displacement, deduced both theoretically and through analysis of

two-dimensional micro-model experiments, were incorporated into models around 5–10 years ago [1–10]: the previous review of this topic for the 25th Anniversary of *Advances in Water Resources* contained an overview of two- and three-phase displacement mechanisms, showed predictions of relative permeability for a simple sandstone, Berea, and provided an assessment of the impact of pore-scale processes on field scale displacement [1].

The major developments over the last ten years have concentrated on models of increasing realism in terms of the pore-scale physics and the development of methodologies to predict multiphase flow and transport properties based on pore-space images. With the advent of more powerful computational resources, the approximation of capillary-control can be relaxed and a number of dynamic network models have been developed recently that incorporate the effects of flow rate, allowing a wider range of displacements to be simulated accurately [60–63].

Later in the paper we discuss the computation of relative permeabilities for mixed-wet carbonates that gives an indication of how network modelling may be applied. The advantages of the technique are that it is possible to make predictions considerably more quickly than direct measurements that typically take several months, it can use small samples, such as drill cuttings and small core fragments that are too small for standard corefloods, and can assess sensitivities, generating, for instance, relative permeabilities for different wettabilities or initial saturations for waterflooding, or for gas injection.

One key component of this workflow is extracting networks from a representation of the pore space. In principle, pores are defined as the larger voids in the rock that are connected by narrower pathways called throats. The pores and throats are assigned effective properties, such as volume, inscribed radius (for the computation of displacement capillary pressure) and shape (that allows wetting phase to reside in the corners, while the non-wetting phase is in the centre). It is also recorded which pores and connected to each other via which throats. There are several techniques employed to do this. Grain-based approaches first identify putative pores as located furthest from grain centres [4]. This works well for clearly granular media and is well suited for pore-space representations derived not from images, but from object-based simulation of grain packing and diagenesis. It works less well for more complex systems, such as many carbonates, where grain identification is difficult.

Erosion-dilation is a rigorous mathematical technique to find the skeleton of the pore space – the skeleton runs through the centres of the pores and throats and defines the topology [64,65]. However, this method suffers from ambiguities given images of finite resolution and has difficulty uniquely identifying pores and their connections. Another method is the maximal ball approach where spheres are grown in the pore space, centred on each void voxel. The largest spheres represent pores, while chains of smaller spheres connecting them define throats [66,67]. This method clearly identifies the larger pores, but tends to identify a cascade of smaller and smaller elements down to the image resolution. At present, network extraction methods can find networks that make reasonable estimates of multiphase properties, as discussed later in this paper, but they still require further verification and do not necessarily provide a unique representation of the pore space independent of image resolution, even in a statistical sense.

Fig. 3 shows networks extracted from the pore space images shown in Fig. 2. Here we have employed the maximal ball algorithm [67]. Despite the approximations inherent in the network extraction, it is an elegant way to represent flow and transport on different scales, with the overall connectivity of the pore space captured by the network, with the smaller-scale (often sub-micron) behaviour described semi-analytically within each network element (pore or throat). This enables computations on much larger samples, spanning a greater spatial range, than direct simulation approaches.

We will now illustrate the use of pore-scale modelling through three examples. This is not intended to be a detailed review of recent results and applications, more it is an indication of the power of the methods demonstrated through illustrative cases. The first example solves for transport directly on the pore space images of different rock samples to determine the nature of dispersion in heterogeneous media. The second is concentrated solely on imaging and does not offer any modelling, but shows how multiphase imaging alone can help answer – directly – important scientific questions: in this case, whether super-critical CO_2 can be trapped as disconnected clusters in the pore space of rock, with application to carbon storage in aquifers. The last example uses network modelling to study relative permeability in mixed-wet carbonates and helps motivate the final section on outstanding problems and issues in this field.

4. Dispersion in heterogeneous media

4.1. Model

Here we simulate flow and transport directly on pore space images using a Stokes solver, applicable for slow (low Reynolds number) flow. The governing equations are:

$$\nabla \cdot \mathbf{v} = 0 \tag{1}$$

$$\mu \nabla^2 \mathbf{v} = \nabla P \tag{2}$$

$$\mathbf{v} = 0 \quad \text{on grains} \tag{3}$$

where $\mathbf{v}$ is the velocity vector, P is pressure, and μ is the fluid viscosity. These equations couple pressure and velocity and are solved using an iterative Semi-Implicit Method for Pressure-Linked Equations (SIMPLE) algorithm [68] employing an algebraic multigrid solver to invert the resultant series of algebraic equations [69]. A velocity of strictly zero is imposed exactly at the pore walls: this enables us to compute the velocity between parallel plates or in simple uniform cross-sections to within machine accuracy using two or more cells across the pore. More details are on the method are given elsewhere [70]. For this application, it would also have been possible to use a lattice Boltzmann technique to solve for the flow field, or to have applied one of a number of open source partial differential solvers, such as the OpenFoam library that has a similar solver to the one used here [71].

Many other authors have simulated flow and dispersion in different porous media using a variety of different methods from network modelling to particle-based simulation directly on pore-space images (see [72–87] for a selection of work in this area). We will not review this research in detail here, except to note that previous studies have demonstrated that given a good representation of the pore space, it is possible to predict measured dispersion coefficients accurately, while explaining how the subtle interplay of molecular diffusion and advection leads to a rich transport behaviour. The emphasis of the work presented in this section will be on what the simulations reveal for highly heterogeneous media – in particular for carbonates, where the pore-level flow field shows significant channelling.

Three different porous materials are studied for comparison purposes: a sand pack, a sandstone (Bentheimer) and a carbonate (Portland limestone), illustrated in Fig. 1 [87]. The computations were performed on a cubic domain containing 300^3 voxels. Details of the images and rock properties are provided in Table 1.

Fig. 4 shows the simulated flow fields. It is evident that for the sand pack there is a relatively uniform flow throughout the domain, but that flow becomes increasingly concentrated in high-velocity pathways for the sandstone and carbonate: in the

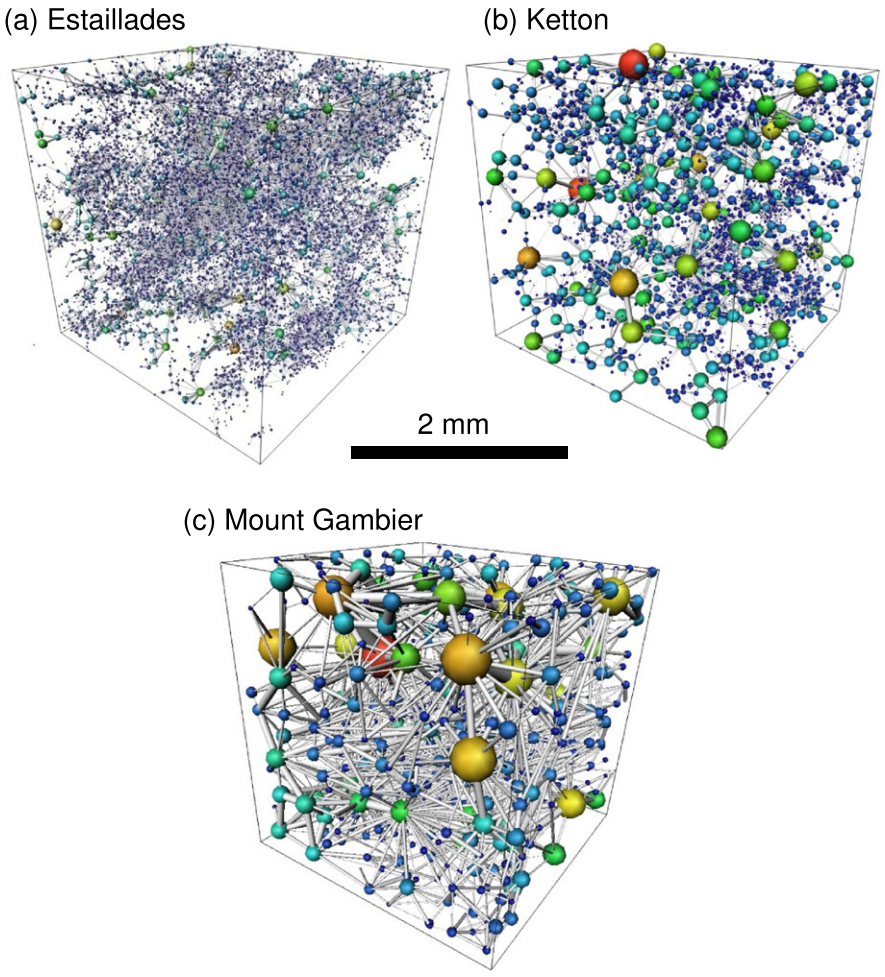

Fig. 3. Pore networks extracted from the images shown in Fig. 2: (a) Estaillades; (b) Ketton; (c) Mount Gambier. For illustrative purposes, only a section of the Mount Gambier network is shown. The pore space is represented as a lattice of wide pores (shown as spheres) connected by narrower throats (shown as cylinders). The size of the pore or throat indicates the inscribed radius. The pores and throats have angular cross-sections – normally a scalene triangle – with a ratio of area to perimeter squared derived from the pore-space image.

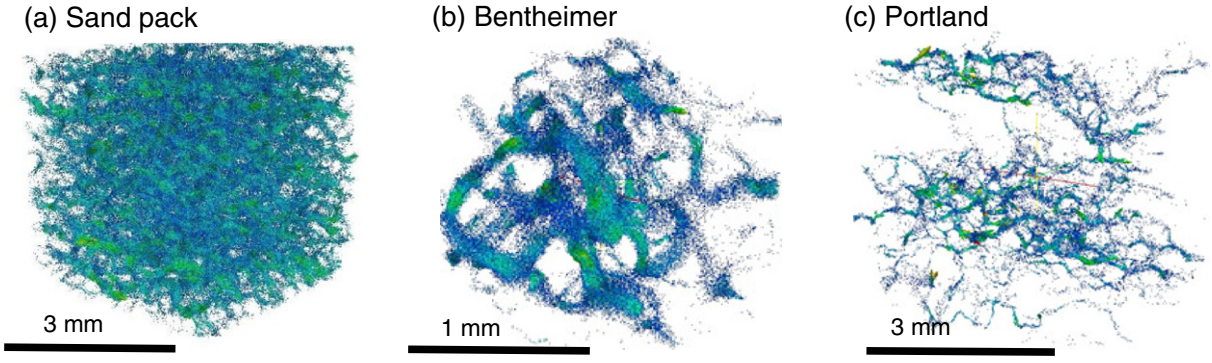

Fig. 4. The flow fields computed on: (a) a sand pack; (b) Bentheimer sandstone; and (c) Portland limestone. Pore-space images of the Bentheimer and Portland, used in this study, are shown in Fig. 1(d)–(f). For the flow computations, a uniform pressure drop is applied across the flow direction with periodic boundary conditions in the other two directions. The colour scale indicates the normalised flow field: blue is slow, while green and red are fast. The flow is computed numerically on a 300^3 image with a resolution of approximately 10 μm for the sand pack, 3 μm for Bentheimer and 9 μm for the limestone.

carbonates most of the pore space is largely stagnant with the flow taken place in just a few channels. It is possible to analyze the distribution of flow velocities: it is found empirically that for low velocities there is an approximate power-law distribution [84,87]. While the average velocity provides a scale for the flow field, there is no characteristic speed, with many slow paths. In terms of transport this represents a power-law distribution of travel times through the domain: conceptually this can be considered the travel times between neighbouring pores [84]. While a full discussion is outside the scope of this paper, the behaviour can then be interpreted and analyzed in the context of continuous time random walks (CTRW) that provide a powerful framework for predicting transport with a wide range of flow velocities [88,89].

We employ a streamline-tracing technique to track the movement of particles through the flow domain. In grid cells that contain no solid boundaries, the method is the Pollock algorithm

used in field-scale streamline-based reservoir simulation [90] where the velocity normal to each face varies linearly with distance from that face. For cells with one or more solid boundary, the tracing of streamlines is more complex. We describe, semi-analytically, the flow field and streamline paths within each grid block, obeying Eqs. (1) and (3) above. The velocity normal to a solid boundary varies quadratically with distance normal to the solid, while the tangential velocity has a bi-linear spatial variation. The details are provided elsewhere [70], but the method allows us to track particles from block to block with no additional errors once the flow field at cell faces is determined.

To simulate dispersion, we also need to include the effects of molecular diffusion. This is accounted for by a random jump of the particles after advection along a streamline. The displacement is given by Mostaghimi et al. [70]:

$$\lambda = \sqrt{6D_m\Delta t} \tag{4}$$

where D_m is the molecular diffusion coefficient (taken, in this work, to be the self-diffusion coefficient of water, 2.2×10^{-9} m^2 s^{-1}) and Δt is the time step size. The coordinates of the particle after diffusion are:

$$x = x_p + \lambda \sin\varphi \cos\theta \tag{5}$$
$$y = y_p + \lambda \sin\varphi \sin\theta \tag{6}$$
$$z = z_p + \lambda \cos\varphi \tag{7}$$

where θ is a random number in the range $(0, 2\pi)$ and φ is another random number in the range $(0, \pi)$ and p labels the position of the particle before diffusion was accounted for.

We track the movement of 50,000 particles initially uniformly distributed throughout the pore space. We take a time step of 10^{-4} s and for each time step move every particle along a streamline and then make a random displacement as described above. We use periodic boundary conditions for the side faces and randomly re-inject, at the inlet, particles that leave the exit face. We define the Peclet number, $Pe = vL/D_m$ where L is a typical pore size, defined as the ratio of the rock volume to the pore-grain surface area [70]. This size is 160, 130 and 290 μm for the sand pack, sandstone and carbonate respectively; our computational domain is between 10 and 20 times larger.

The longitudinal dispersion coefficient is computed by calculating the variance of the distance travelled by particles in the main direction of flow:

$$D_L = \frac{1}{2}\frac{d\sigma^2}{dt} \tag{8}$$

where σ^2 is the variance of the particle displacement, x_i:

$$\sigma^2 = \left\langle [x_i(t) - \langle x_i(t)\rangle]^2 \right\rangle \tag{9}$$

4.2. Results

Fig. 5 shows the computed concentration profile as a function of distance for dispersion through the three porous media studied. Technically what are shown are propagators – that is the probability of displacement at a given time: particles that have different starting locations are assigned a zero displacement initially. The results are compared to NMR measurements on similar rock samples [91,92] and show good agreement. This demonstrates that with a good image of a representative rock sample, even for a carbonate, pore-scale simulation can make quantitative predictions: in this analysis there are no fitting parameters. For unconsolidated media, several other authors have provided better predictions of propagators and dispersion coefficient from direct simulation – usually using the lattice Boltzmann approach – on pore-space images. By reproducing the pore structure exactly – instead here we compare a sand pack with experiments on a bead pack, with more rounded

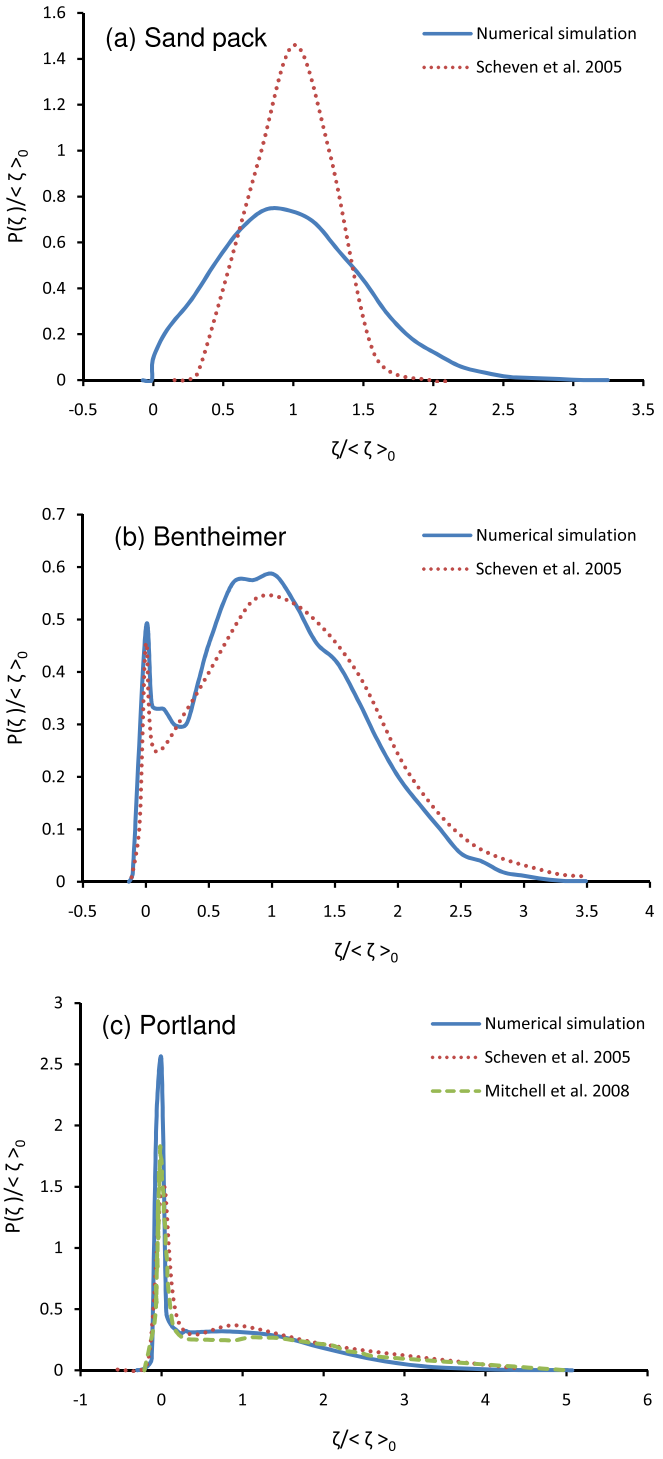

Fig. 5. Predicted propagators for transport in the three rock samples whose flow fields are shown in Fig. 4. The propagator is the probability $P(\zeta)$ of displacement ζ in the main direction of flow. The predictions are compared to NMR measurements Scheven et al. [91] and Mitchell et al. [92]. The Peclet number is around 200 in both the simulations and the experiments with a mean flow velocity of approximately 1 mm/s and a displacement time of 1 s. The distance axis is scaled so that movement at the average velocity has a displacement of 1. (a) Sand pack. With a rather uniform flow field, we see a Gaussian-like spread of the plume around a mean position governed by the average flow. (b) Bentheimer sandstone. Some of the plume is retarded with an elongated tail. (c) Portland limestone. Most of the plume is effectively stagnant and a very dispersed profile. This cannot be captured – even qualitatively – by traditional advection–dispersion models.

grains – excellent agreement can be obtained [75,76,81,93,94]. We obtain good predictions where our images represent the rock being studied experimentally: Bentheimer and Portland. For Portland, we do not resolve some of the smallest pores, below the resolution of the scan. The successful prediction of the propagators suggests that these small pores do not significantly affect the behaviour.

More interesting though is what is revealed by the simulations about the generic nature of dispersion. For the unconsolidated system, where the flow field (see Fig. 4) is relatively uniform, the behaviour is as expected: the peak of the plume is centred at a normalised displacement of 1 with a Gaussian-like spread about the mean. This transport is broadly consistent with a one-dimensional solution of the advection–dispersion equation in a homogeneous medium [95]:

$$\frac{\partial C}{\partial t} + v\frac{\partial C}{\partial x} = D_L\frac{\partial^2 C}{\partial x^2} \tag{10}$$

where C is the concentration and D_L is defined by Eq. (9). Even for unconsolidated media, there are significant deviations from purely Fickian behaviour (that is a concentration profile given by a solution to Eq. (10)) at early time [75,76,81,93]. However, for the sandstone we see a qualitatively different profile: there is a peak in the concentration near zero, representing particles in stagnant regions of the pore space that have barely moved. At larger displacement there is a dispersed profile with a wide range of movement consistent with a wide range of local flow velocities.

The concentration profile for the carbonate is very different from any prediction from the advection–dispersion equation (see Fig. 5): the peak concentration is near zero, indicating that most of the particles are stuck in stagnant regions of the pore space with a few that see the fast-flowing regions, giving a very elongated leading edge of the plume. The physical explanation for this behaviour is the power-law distribution of travel times between pores – there is no typical transit time and hence a formulation based on Eq. (10) that pre-supposes a typical mean displacement and a variation around this displacement is flawed [84].

Eventually, molecular diffusion will allow particles to diffuse out of slow-flowing regions; in time every single particle will sample the entire flow field – both slow and fast – and a so-called asymptotic limit is reached where Eq. (10) is valid. In this regime, D_L, defined by Eq. (8), no longer changes with time and indeed a concentration profile is seen with a peak at a dimensionless displacement of 1 and a Gaussian profile around this mean with a variance related to D_L [95]. This asymptotic dispersion coefficient is plotted in Fig. 6 as a function of Peclet number. We are able to predict measurements on unconsolidated media [96–104] within the scatter of experimental measurements in the literature.

In the intermediate Peclet number regime, $300 > Pe > 5$, we observe an approximate power-law relationship between dispersion coefficient and Pe [95]. The exponent is a function of the heterogeneity of the porous medium – it is 1.2 for sandstones and sand or bead packs and 1.4 for the carbonate sample studied. In addition the magnitude of D_L is larger for more heterogeneous media with a wider range of flow velocities. The physical origin of this power-law is the power-law distribution of travel times and the exponent can be predicted from the flow field using CTRW theory [84,87,89]. The dispersion coefficient increases with time as the particles sample the flow field with both slow and very fast regions; eventually molecular diffusion allows all particles to sample the flow field uniformly and an asymptotic limit is reached, but the spread of the plume at this point is related to the scaling of the distribution of local travel times. A detailed analysis of the flow field in Portland stone studied confirmed a power-law distribution of transit times across grid blocks that is related to both the increase in measured dispersion coefficient with time and the non-linear scaling of dispersion coefficient with Peclet number [87].

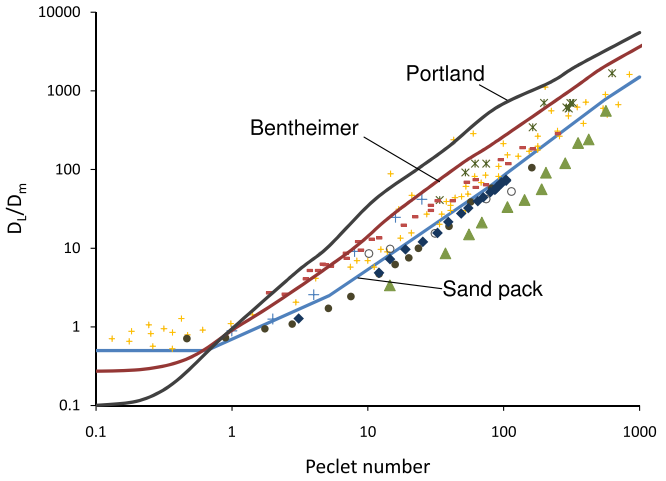

Fig. 6. Predicted asymptotic dimensionless dispersion coefficient (D_L/D_m where D_L is the dispersion coefficient in the overall flow direction and D_m is the molecular diffusion coefficient) as a function of Peclet number for the different rock types indicated (lines). The points are experiments on bead packs and other unconsolidated media taken from the literature (small + [96], filled circles [97], filled triangles [98], open circles [99], diamonds [100], × [101], stars [102], large + [103], – [104]). In the intermediate Peclet number regime there is an approximate power-law relationship between dispersion coefficient and Peclet number with an exponent that is related to the power-law variation of travel times between pores.

4.3. Discussion

This first example implies that a contaminant plume may be held back in slow-flow regions of the pore space in highly heterogeneous media, with most of the solute stranded in stagnant regions with a long, fast-flowing leading edge. Eventually, particles diffuse out of stagnant regions and sample the whole field and an asymptotic behaviour is attained, consistent with the advection–dispersion Eq. (10), universally used in field-scale contaminant transport simulations.

It is possible to estimate how long it takes for this asymptotic limit to be reached if we assume that there are significant regions of the pore space with essentially a negligible flow velocity: it is simply the time taken for a particle to sample the heterogeneity of the medium by molecular diffusion. If this heterogeneity is present on a length scale l – this is effectively the size of a representative element of volume – the diffusion time is $l^2/2D_m$ [84]. For a sand or bead pack this is a typical pore length, since there are no significantly larger-scale correlations in either the pore-space geometry or the resultant flow field. In our case, using the self-diffusion coefficient quoted previously and a typical pore length of 100 μm we find a typical time of around 2 s; as we see in Fig. 5, after 1 s we already observe the development of a plausibly Gaussian plume. For the sandstone and carbonate the flow field indicates that there is channelling on the scale of the simulation domain of a few millimetres – if we take $l = 2$ mm we find a diffusion time of around 1000 s. For the representative flow velocity of around 1 mm/s used in our simulations, this represents an average displacement of 1 m. What this means physically is that while the average solute particle has moved 1 m, those that are slowest moving have only managed to diffuse around 2 mm to escape – finally – into a fast flowing region. If we consider transport in a flow domain that is homogeneous on all scales beyond 2 mm then, eventually, an asymptotic regime is achieved once the plume has travelled many metres. While in carefully-controlled experiments on selected, macroscopically homogenous cores, the emergence

of a truly asymptotic dispersion regime may be possible – and, thanks to the use of periodic boundary conditions – is feasible to simulate, it is unlikely that the real systems of interest – oil fields, saline aquifers used for carbon dioxide storage and contaminated sites – are homogeneous on these scales. As the plume moves, it is likely to encounter heterogeneity with structure of different size containing associated slow flow regions with even larger characteristic times for escape, delaying portions of the plume and rendering consideration of an asymptotic dispersion coefficient to be used in an advection–dispersion equation largely useless. This concern applies even for slow flows at low Peclet numbers: while diffusion may lead to complete mixing at the pore scale, at late times, the plume will experience larger-scale heterogeneity through which diffusion will still be slow compared to advection. This is manifest, at the aquifer scale, by an apparent dispersion coefficient that increases approximately linearly with the distance the plume has travelled [105]. The inability to determine a unique time-and-space independent dispersion coefficient poses a challenge for larger-scale modelling; near the end of the paper we discuss possible upscaling techniques to incorporate the effects of pore-scale heterogeneity in field-scale simulation.

Consider one application where this work may be applied: CO_2 storage, where the injected CO_2 may dissolve into the resident brine. This CO_2-laden brine is denser than the native brine and sinks. This sets up a buoyancy-driven flow with downwards moving fingers of dense brine, while fresh brine contacts the CO_2-phase, leading to convective mixing [106–110]. Previous treatments of this problem have assumed that the advection–dispersion equation is valid for this process at the field scale (see, for instance [106,107]); the authors employed the standard macroscopic description of transport. If, however, the peak of the plume moves slower than would be predicted using a conventional model, the establishment of a buoyancy-driven flow may be delayed, making this mechanism for long-term safe storage less effective than considered previously. Similar considerations pertain to the use of pumping strategies to remove contaminant from groundwater, or mixing of miscible gas and oil in enhanced hydrocarbon recovery – again this analysis suggests a very long, slow tail of solute making complete removal or recovery very difficult.

This work could readily be extended to study coupled processes, such as reaction, including precipitation and/or dissolution of the pore space. This could be used to provide a rigorous pore-scale basis for field-scale simulations of reactive transport. The important and exciting feature of this work is that conceptually simple numerical modelling through three-dimensional images of the pore space yields fresh insight into these fundamental processes.

5. Imaging of residual super-critical carbon dioxide

One possible method to reduce atmospheric emissions of CO_2, and hence to mitigate climate change, is carbon capture and storage, where CO_2 from fossil-fuel burning power stations and other industrial sites is collected, transported and injected deep underground [111]. Storage sites include coal seams, depleted hydrocarbon reservoirs and saline aquifers. Saline aquifers provide the largest likely storage potential and are geographically widespread. The principal design criterion for an aquifer injection scheme is to ensure that the CO_2 remains underground for hundreds or thousands of years so that it will not contribute to climate change.

When the CO_2 is injected there are four mechanisms by which the CO_2 remains trapped underground [111]. The first is when the buoyant CO_2 is trapped underneath low-permeability caprock through which it cannot flow, or flows so slowly that it takes many millennia to escape. This is a reliable mechanism for well-characterised aquifers where there is known to be a good trap for the CO_2, and may be suitable for hydrocarbon fields where oil and gas have already been contained for geological time. However, in many other settings it is not clear that there is intact low-permeability rock over the large distances that CO_2 might migrate – likely to be many 10 s km for large storage projects. In this case other processes need to be used to ensure safe long-term storage. The second mechanism is dissolution: here some CO_2 dissolves in the resident brine – as discussed in the previous section – and the denser CO_2-laden brine sinks [108]. However, in many field settings this is very slow, taking hundreds or thousands of years to remove a mobile, buoyant plume that may, in the meantime, have escaped to the surface [106–109]. Furthermore, our dispersion analysis implies that the mixing required to establish significant dissolution may be even slower than predicted from traditional mathematical models. The third and safest storage mechanism is mineral precipitation where the acidic CO_2-rich brine reacts with the host rock to produce solid carbonate [112]. This process, however, relies on a favourable mineralogy of the rock and can also be extremely slow, taking thousands to millions of years to sequester a significant fraction of the injected CO_2 [112].

The final sequestration mechanism is capillary trapping [113–116]. As the CO_2 moves through the aquifer it is displaced by brine. This displacement is likely to leave behind a trail of trapped, residual CO_2. This process is analogous to the trapping of oil or gas in waterflooded hydrocarbon fields. If CO_2 is the non-wetting phase, brine will preferentially fill the narrower regions of the pore space, flowing through wetting layers, stranding CO_2 in wider pores in a process called snap-off [117–119]. This results in a large fraction of the pore volume being occupied by residual CO_2 surrounded by brine. If brine is not the wetting phase, there is less trapping, since CO_2 will be displaced by piston-like advance, the brine will not preferentially fill the smaller regions of the pore space; there is no layer flow and snap-off [119]. It has been hypothesized that this process could rapidly and effectively trap a significant fraction of the CO_2 within a few years, while limiting its spread, preventing escape, assuming that the rock is non-wetting to CO_2 [114]. Furthermore, the process could be engineered through the artificial injection of brine extracted from elsewhere in the aquifer [116].

Promising though capillary trapping is as a potential storage mechanism, there has been, to date, no direct evidence of this process at the pore scale. Coreflood experiments have suggested that significant amounts of CO_2 could be trapped, although with a residual saturation lower than in analogue oil/water systems that are strongly water-wet [120]. However, some experiments have measured the CO_2-brine-solid contact angle and capillary pressures that indicate neutrally or even CO_2-wet conditions, implying little trapping [121–123].

Residual non-wetting phase has been imaged using micro-CT scanning previously, but only on analogue systems at ambient conditions where the porous medium was strongly water-wet [124–128] or oil-wet [129,130]. In this section we use micro-CT imaging to image trapped supercritical CO_2 in the pore space of a sandstone, demonstrating that capillary trapping could be an effective storage process. Silin et al. also imaged fluid distributions after CO_2 injection – they did not consider trapping – using a synchrotron source, but the images were of rather poor quality [131]. Our study is a direct use of imaging technology without associated pore-scale modelling, although in future, modelling this process at the pore scale could serve to validate pore-scale simulators and understand the pore-scale dynamics of trapping.

5.1. Experiment

The experimental apparatus is essentially a miniature version of a standard Hassler sleeve used in routine core analysis in the oil industry [132]; further details are provided elsewhere [28]. The

key difference is that to contain the fluids at high pressures and elevated temperatures, rather than use an X-ray opaque steel sleeve, the core holder is constructed from carbon fibre. The carbon fibre is thin, allowing the core to be placed close to the X-ray source in a micro-CT scanner, and is transparent to X-rays. The core itself has a diameter of 5 mm and length 9 mm and is imaged at a resolution of approximately 13.7 μm in these experiments. The core is wrapped in aluminium foil to prevent escape of the CO_2, that is then contained in an elastomer (Viton) sleeve, while the carbon fibre assembly contains a confining fluid to compress the sleeve to maintain pressure and temperature.

The rock is a Doddington sandstone that is 98 wt.% α-quartz, 2 wt.% K-feldspar with traces of kaolinite (measured by X-ray diffraction on a Philips PW1830 diffractometer) and a well-connected pore space. The fluids are maintained at a pressure of 9 MPa and a temperature of 50 °C; these conditions are representative of a storage aquifer at a depth of around 900 m and represent supercritical conditions for CO_2 [28].

The core is initially saturated with brine. Then CO_2 is injected. This is a primary drainage experiment representing the initial injection of CO_2 into the aquifer. An initial saturation of approximately 44% is established. Then brine is injected. This brine is already saturated with CO_2 at the experimental conditions using a stirred reactor [28]. That exact equilibrium is reached is vitally important; if the brine is undersaturated with CO_2, some CO_2 will dissolve, leading to an under-estimate of residual saturation. The displacement of CO_2 by CO_2-saturated brine represents the likely displacement process in the middle of a large CO_2 plume where there has been sufficient time for chemical equilibrium between the phases to be established. Approximately 50 pore volumes of brine are injected at a low flow rate representing a capillary number $C_a = \mu q/\sigma$ of around 2×10^{-5} where μ is the fluid viscosity, q is the Darcy velocity and σ is the CO_2-brine interfacial tension. The core is scanned dry to image the pore space, when saturated with brine, after CO_2 injection and after brine re-injection. As mentioned previously, the raw micro-CT images were cleaned of ring artefacts [25]. Salt-and-pepper noise was removed with an anisotropic diffusion filter [133] and the phases were then segmented according to their CT contrast using multi-thresholding based on Otsu's algorithm [27].

5.2. Results

Fig. 7 shows the distribution of trapped CO_2 in the pore space. The pictures are two-dimensional cross-sections of a three-dimensional image. Here we capture both the pore structure of the rock and the fluids simultaneously. The images directly confirm that CO_2 can be trapped in the pore space, surrounded by brine. Fig. 8 illustrates some of the trapped clusters captured in three dimensions; it is evident that clusters of all size are present, from small blobs in the centre of a single pore to ramified, extensive ganglia spanning several pores.

Table 2 compares the average saturation measured by summing the volume in all the trapped clusters with an analogue experiment on the same core but with *n*-octane as the non-wetting phase. In addition the results are compared to corefloods on larger rock samples (diameter 3.8 cm and length 7.5 cm). The results are consistent between the micro-CT scans and corefloods and indicate that while there is significant trapping of the CO_2, the residual saturation is lower than that measured on analogue oil-brine systems that are assumed to be strongly water-wet. The suggestion is that CO_2-brine systems are less strongly water-wet, suppressing trapping through wetting layer flow and snap-off and leading to lowered residual saturations [118–120]. In a more detailed analysis we have compared the distribution of trapped cluster size with an analogue strongly water-wet system [28]. The results show that with CO_2 there are fewer small clusters, confirming that the amount of snap-off is reduced, but many larger ganglia are present, providing a large surface area for dissolution and reaction.

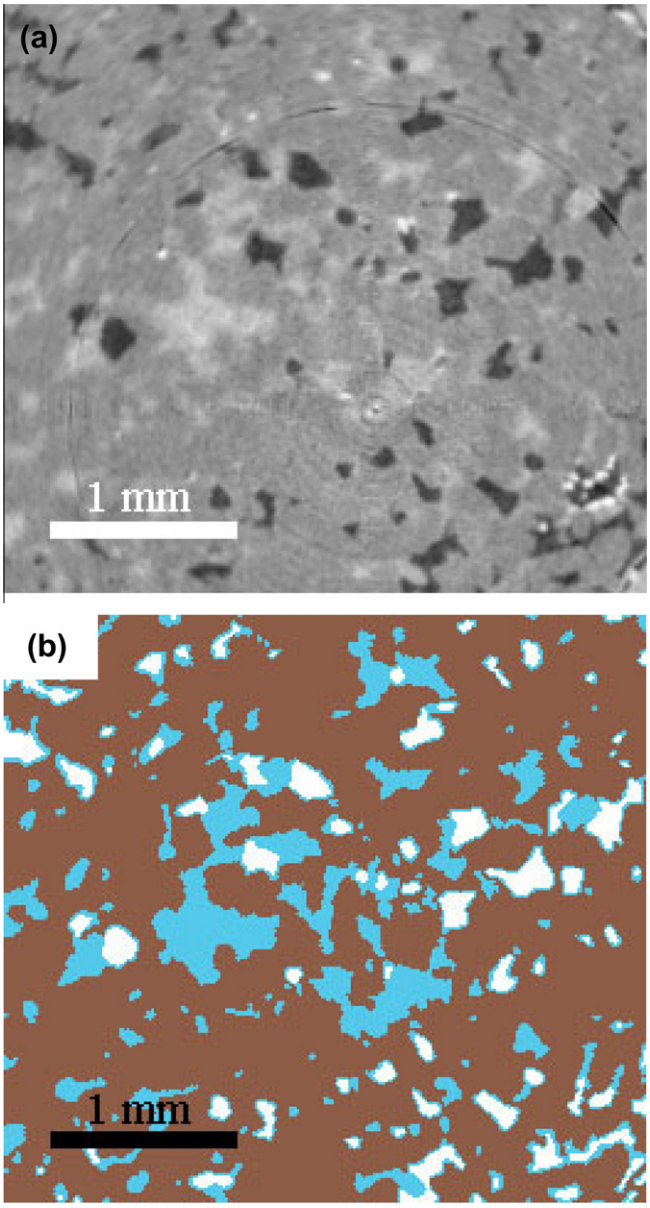

Fig. 7. Images of CO_2 after waterflooding with CO_2 saturated brine, showing the trapped supercritical CO_2 clusters. The picture is a two-dimensional cross-section through a three-dimensional image; the area shown is 3.434 mm × 3.144 mm ≈ 10.80 mm^2 (261 × 239 voxels). (a) A raw grey-scale image: supercritical CO_2 is black, brine is light grey and sandstone is dark grey. The few white areas are minerals with high X-ray absorption. (b) The same slice with phases segmented. Supercritical CO_2 is white, brine light blue and rock is brown.

5.3. Implications and future work

This work provides compelling evidence that capillary trapping could be an effective storage strategy; it certainly will allow CO_2 to be trapped locally and occupy a significant fraction of the pore space. This work needs to be coupled with field-scale simulation to determine the effectiveness of the storage design, since the amount of CO_2 trapped will depend on both the local trapping efficiency and the fraction of the volume of the aquifer – at the large

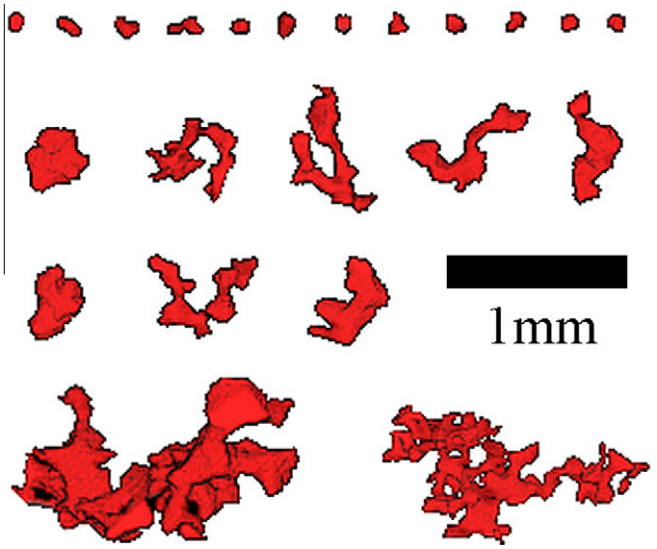

Fig. 8. Images of CO_2 after waterflooding with CO_2 saturated brine showing selected trapped clusters of different size.

scale – contacted by CO_2. We have studied only a single pressure and temperature: the variation in the amount of trapping as the reservoir conditions vary, particularly as the CO_2 density increases, is not known. Furthermore, this work is confined to a single homogeneous quarry sandstone of high porosity and almost pure silica content. The effects of clays and other mineralogies present in reservoir samples needs to be investigated. It is possible that carbonates may result in significantly less water-wet conditions, because of a significantly different surface chemistry. Indeed it is possible that they could be neutrally to CO_2-wet, resulting in very low residual saturations and precluding capillary trapping as an effective trapping mechanism. Last, injection is also likely to be combined with geochemical reaction, both to dissolve or precipitate carbonate: the study of these coupled processes is an interesting topic for future study.

The degree of trapping, as already mentioned, is governed by the interplay of snap-off and piston-like advance. Current network models use parameterized models to describe piston-like pore filling [2,7]: these experiments could provide a challenge to these models enabling the development of improved correlations to capture correctly the amount of trapping in media that are not strongly water-wet.

This is an example of where pore-space imaging alone provides insight into important multiphase processes in porous media. It is however, just one application of this novel technology, simply studying fluid distributions at the end of a displacement on a permeable sandstone at a relatively poor resolution compared to the best modern scanners. With improvements in image resolution and the speed with which images can be captured, it is likely that the dynamics of multiphase flow for less permeable samples will be captured, providing unparalleled insight into porous media processes [10,13].

6. Relative permeability of mixed-wet carbonates

6.1. Significance

In this final section we present a study of relative permeability and wettability in carbonates. It is estimated that more than half the world's remaining recoverable reserves of conventional oil are contained in carbonate reservoirs, many of them in the Middle East [134]. These reservoirs pose a challenge both for reservoir management and characterisation. The pore space is heterogeneous on many scales, with pore sizes ranging from around 0.1 μm to mm or cm-sized vugs, combined with dramatic spatial variations in local porosity, permeability and pore connectivity [36]. In general, carbonate rocks exposed to crude oil are oil-wet, or mixed-wet, where there are regions of the pore space that are oil-wet with other connected patches that remain water-wet. These reservoirs are also generally extensively fractured.

Waterflooding the reservoir to displace oil works by two very distinct mechanisms [135]. The first is viscous displacement through the matrix (the unfractured rock): here the recovery is controlled by the relative permeability and specifically the relative permeabilities near the residual oil saturation. However, if the fractures have a much higher permeability than the matrix, the injected water flows through the fractures, and displacement of oil in the matrix is controlled by capillary imbibition and gravity drainage. If capillary forces are significant, then the overall recovery is determined not by the residual oil saturation, but the saturation when the capillary pressure reaches zero. If the rock is mixed-wet this will lead to a much higher remaining oil saturation; if oil-wet there may be no spontaneous imbibition at all. Furthermore, in mixed-wet media, the rate of imbibition is much slower than for water-wet systems with the same pore structure, since the water relative permeability is low, representing poor connectivity of the wetting phase [7,136]. The recovery in a field setting is a complex interaction of field-scale heterogeneity – in particular the connectivity of the fracture network – combined to small-scale displacement efficiency with capillary, viscous and gravitational forces all playing a role. The starting point for a thorough assessment of recovery and injection design is good relative permeability and capillary pressure data, but reliable measurements on representative core samples are often scarce. Pore-scale modelling offers the possibility of generating data on many samples combined with an assessment of uncertainty or sensitivity to variations in rock type and wettability, benchmarked against good quality experimental data.

6.2. Methodology

In this section we will show some example network modelling results for carbonates and compare to measurements on a reservoir sample from the Middle East. We will use the results to illus-

Table 2
Porosities and saturations measured using micro-CT scanning and by coreflooding.

	Porosity CT (%)	Porosity He* (%)	CO_2 saturation Micro-CT (%)	CO_2 saturation Coreflood ** (%)	Oil saturation Micro-CT*** (%)	Oil saturation Coreflood** (%)
Primary drainage	20.5	20.7	48.0 (Initial)	50 (Initial)	Not measured (initial)	44 (Initial)
Waterflooding	20.8	20.7	24.9 (Residual)	25 (Residual)	35.0 (Residual)	35 (Residual)

* Measured via Helium pycnometry on a larger core sample of the same rock [128].
** Measured with the porous plate method on a Berea sandstone core (porosity = 0.22 and brine permeability = 4.6×10^{-13} m^2) [120].
*** Measured in a similar micro-CT experiment with the same rock with n-octane at ambient conditions [125].

trate a possible workflow for characterising multiphase flow properties in such samples and discuss, briefly, generic features of the results and their implications for recovery. This section will explore the possibilities and difficulties associated with multiphase flow predictions in carbonates.

The methodology for predicting relative permeability has already been outlined [36,136], while the sensitivity of relative permeability to rock type and wettability have been explored in a few samples [137]. However, this work has been limited in practice to the difficulty of coupling detailed images – often acquired at different scales – and the modelling of multiphase flow. The steps are as follows:

(1) *Image acquisition*: As discussed previously, standard micro-CT scanning has a 1000-fold range in image size, typically resolving the pore space at the scale of a few μm on a sample a few mm across. In many carbonates, there is significant connected pore space of a size less than a μm, combined with core-scale heterogeneity that makes a description of the pore space at the mm scale unrepresentative. This is evident in the images shown in Fig. 1, where micro-porosity in some of the samples could not be resolved while simultaneously capturing the larger pores. What is required is a multiscale approach that combines whole core analysis, micro-CT imaging and higher resolution techniques, such as FIB/SEM [36]. Another approach is to generate a statistical or object-based model, discussed below, based on high-resolution two-dimensional images, from, for instance, SEM.

(2) *Model building*: A representative model of the core, or sections of it, is needed for simulations of multiphase displacement. This can simply be a single micro-CT image (this is what we will do in this section to illustrate the methodology), but for many carbonates, as discussed already, this will provide a rather inadequate representation of the pore space. Another approach is to use a high-resolution two-dimensional image as a template for the construction of a three-dimensional image through statistical techniques. Most of these methods now employ multiple point statistics, or some form of pattern recognition, to preserve the connectivity of the pore space [35]. Alternatively, images taken at different scales can be merged, or combined with discrete modelling of grains and diagenetic features, providing a multiscale representation of the pore space [36]. If multiphase flow is computed directly on these images, then all that is required is a final image of appropriate size and resolution. If network modelling is employed, then a topologically representative network is extracted from the image; again this network may explicitly account for porosity apparent at different length scales [35,138].

(3) *Simulating multiphase flow*: There are several different approaches to be used here, including direct (typically lattice Boltzmann) simulation of displacement on different subsections of the rock. The other approach is network modelling, described before, where displacement in each element (pore or throat) is described semi-analytically. This latter approach will be used in this section.

(4) *Upscaling to the core scale and beyond*: Current simulation technology is limited to direct simulation of multiphase flow properties on images of a few hundred voxels on each side, representing samples at most few mm across. Pore-scale modelling allows larger models to be represented, containing the equivalent of a few million pores and a sample approaching the core scale. In any event, however, the simulations are on small rock samples, well below the size of a whole reservoir core and certainly smaller than a reservoir simulation grid block – typically 10–100 s m across – for which the relative permeability and capillary pressure are input for field-scale modelling. The simple-minded approach is to assume that the small-scale properties are representative at the larger scale and use these directly in field-scale simulation. However, the availability of images on different samples and the ease of making multiphase flow predictions encourages a more rigorous approach where the properties computed at different locations are averaged. This is still the topic of active research and will be discussed in Section 7.

In this work we will illustrate a simplified version of this methodology, where we assume that the micro-CT images capture the larger voids and their connectivity adequately. In this work we take three quarry carbonates: Estaillades, Mount Gambier and Ketton, shown in Figs. 1 and 2.

We extract networks from these images using the maximal ball method outlined previously [67]. Table 3 provides the statistics of the extracted networks, while Fig. 3 depicts the networks themselves. Mount Gambier has a much more connected pore space with a higher coordination number (average number of throats connected to each pore) of around 7 compared to Ketton and Estaillades that have coordination numbers of approximately 3; Estaillades also has a significant number of isolated elements – it is possible that these pores and throats are connected through micro-porosity that we failed to image.

We then simulate capillary-controlled displacement: the medium is assumed to be filled initially with wetting phase (water) and oil is injected. This primary drainage process, where we assume that the rock is strongly water-wet, represents primary oil migration into the reservoir. We then model waterflooding. Where oil has been in direct contact with the rock surface, we allow the contact angle for waterflooding (the advancing contact angle) to be assigned an arbitrary value. In the examples we present we have no *a priori* way to know contact angle on a pore-by-pore basis: the parameters we use are shown in Table 4. In previous work, the average contact angle and oil-wet fraction (that is the fraction of the pores and throats that are assigned contact angles greater than 90°) has been adjusted to match the measured residual oil saturation or Amott wettability indices [7]. We discuss later how contact angles could be estimated directly from an analysis of images taken during waterflooding for samples of interest. While the assignment of contact angle appears to be a major limitation of a predictive approach, it is possible to assign plausible values to match available data and then explore the sensitivity of the predicted relative permeability to changes in pore structure, initial water saturation and wettability [137]. Indeed it is in investigating these sensitivities that pore-scale modelling has its greatest value, predicting properties for cases that are difficult to explore in a feasible time-frame from coreflood experiments.

6.3. Results

Fig. 9 shows the computed primary drainage and waterflood capillary pressures for the three samples studied. In this example 25% of pores and throats, chosen at random, containing water remain water-wet, while 75% (the oil-wet fraction) have a contact

Table 3
Network properties for the three carbonate samples studied.

	Ketton	Estaillades	Mount Gambier
Number of pores	4673	59305	22665
Number of throats	7341	90682	84593
Number of isolated elements	607	20301	257
Volume (mm^3)	18.7	19.3	31.3
Coordination number	3.08	3.03	7.41

Table 4
Fluid properties and contact angles used in the simulations.

Initial contact angle (degrees)	0
Interfacial tension (mN/m)	48.3
Water-wet contact angles (degrees)	0–60
Oil wet contact angles (degrees)	100–160
Oil-wet fraction	0.5 and 0.75
Oil viscosity (mPa s)	0.547
Water viscosity (mPa s)	0.4554

angle assigned at random between 100° and 160°. Table 4 shows the contact angles and interfacial tensions used in this study.

Fig. 10 shows the computed waterflood relative permeabilities for the cases shown in Fig. 9. The measured relative permeability on a reservoir carbonate from the Middle East at prevailing wettability conditions is also shown [139]. It can be seen that the same generic behaviour for the oil relative permeability is observed: the comparison is not predictive, since no direct images of the reservoir sample were available and we have guessed the wettability. We see similar trends to the experimental data using the Mount Gambier network and a fractional wettability of around 0.5. The reservoir sample has a much lower permeability, 11 mD, than our networks (Table 1). Previous work – using much smaller networks – has indicated a predictive capability where carbonate images are available and there is some independent assessment of core-scale wettability [136].

In all the cases we see a low residual oil saturation. The mixed-wet nature of the system (assigned in the model and inferred from the experiment) allows oil to be connected in thin layers, sandwiched between water in the corners of the pore space and water in the oil-wet centres of the pores. The slow drainage of these layers allows low residual saturations to be reached, but the oil relative permeability is also very low [7]. The water relative permeability at low water saturation is also small: waterflooding first invades the smaller water-wet pores and throats that have a poor conductance and which are not necessarily well connected in the pore space. Then, when the waterflood capillary pressure becomes negative, the nature of the displacement changes and now the larger oil-wet pores are filled. This leads to large changes in water saturation, but the water only becomes well connected once these water-filled pores and throats span the system. We observe that for the well connected system – Mount Gambier – the water relative permeability rises faster than for networks with lower coordination number, since it is easier for the water to span the system in this case. The experiments show similar behaviour to

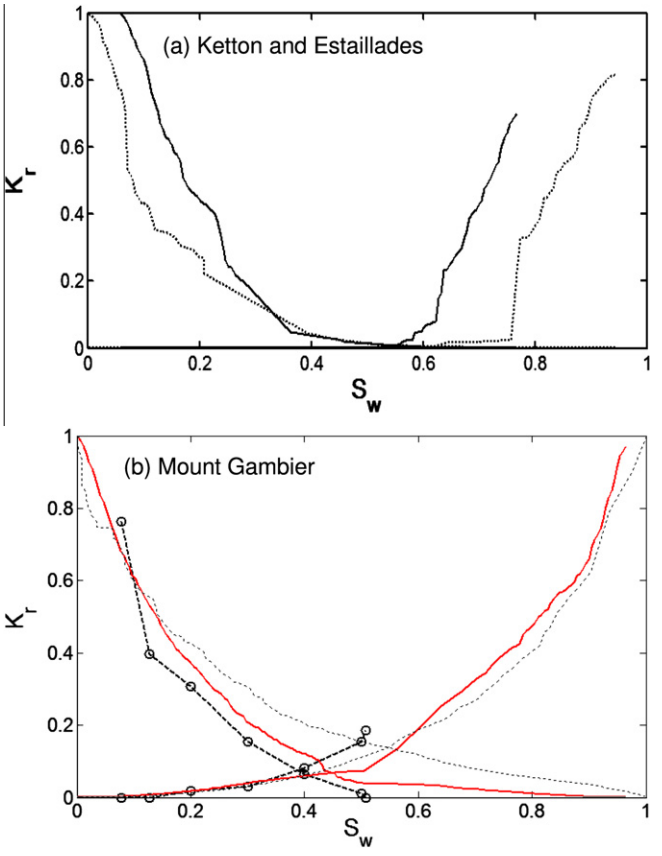

Fig. 10. Waterflood relative permeabilities computed for different networks. (a) Ketton (dashed lines) and Estaillades (solid lines) with an oil-wet fraction of 0.75. (b) Mount Gambier (red line is an oil-wet fraction of 0.5; dashed line is an oil-wet fraction of 0.75) compared to steady-state measurements on an aged reservoir core from a giant carbonate field in the Middle East [139] (dashed lines with circles) (For interpretation of the references to colour in this figure legend, the reader is referred to the web version of this article.).

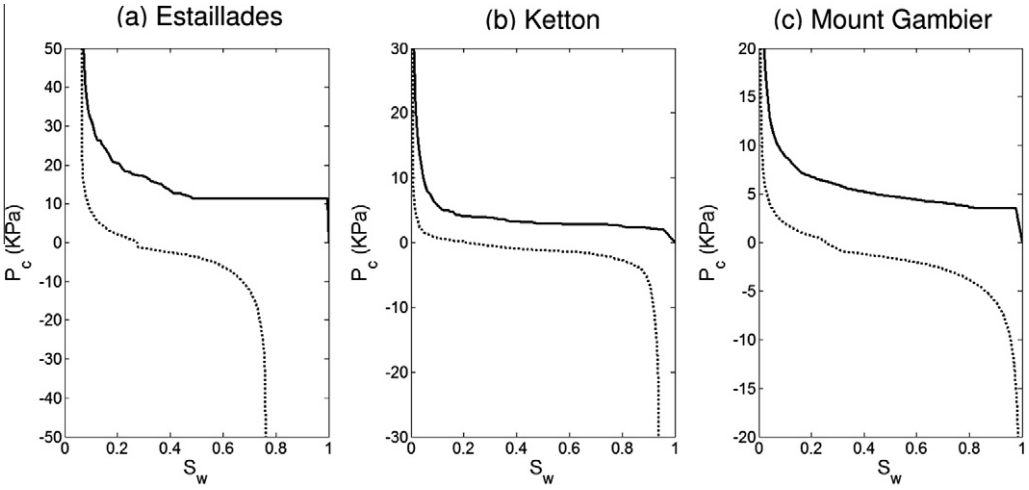

Fig. 9. Primary drainage (solid line) and waterflood (dashed line) capillary pressure predicted on (a) Estaillades, (b) Ketton, and (c) Mount Gambier networks. We assume that the samples are mixed-wet with an oil-wet fraction of 75%; approximately 25% of the moveable pore volume is displaced by spontaneous imbibition where the capillary pressure is positive during waterflooding.

Mount Gambier, indicating a well connected pore space with a large coordination number. We predict a lower residual saturation, but this is achieved through slow oil layer drainage at a large negative capillary pressure, which is difficult to impose in the steady-state experiments.

In all three cases the predicted oil relative permeability is a close match to the experimental measurement. We have assumed that the samples are mixed-wet. As a result, oil remains connected through most of the displacement in the smaller pores and in layers in the larger pores whose centres are water-filled. This behaviour is captured adequately and is most sensitive to the overall wettability of the sample [137]. In contrast, our predictions of water relative permeability for the two low-coordination number samples are very different from the experimental measurements, with an extremely low relative permeability at low and intermediate water saturation, followed by a rapid increase when water becomes connected through the centres of the pore space. We have ignored micro-porosity, which was not captured in our micro-CT scans. This micro-porosity is likely to remain full of water, but does provide connectivity and may result in rather larger water relative permeabilities than predicted here. Furthermore, this means that our assumed initial (and irreducible) water saturation is close to zero. Another potential source of inaccuracy is the network size: for the two less well connected networks, the predicted relative permeabilities feature sudden jumps related to the poor connectivity of the phases. It is likely that networks with more pores and throats, representing a larger sample, would give smoother and more reliable predictions.

Note that to make these predictions we need to capture the effects of layer flow of both water and oil. This requires effectively a high-resolution simulation at the sub-pore level. This can be achieved through network modelling, where the fluid configurations are idealised with infinite resolution in each pore and throat, but poses a challenge to direct simulation approaches that would require grid refinement in the smallest pore spaces to allow such complex fluid distributions to be captured.

6.4. Field-scale implications

The field-scale consequences of these properties can only be properly judged through reservoir simulation, where relative permeabilities and capillary pressures for the rock types and initial saturations observed or inferred in the field are input into larger-scale simulation, coupled with a detailed description of the geology, including the presence of faults and factures. A discussion of this is outside the scope of the paper, but the multiphase properties themselves indicate likely recovery trends and can act independently as a guide to reservoir management. Again this is one of the valuable contributions from pore-scale modelling, allowing direct insight into recovery processes as a rapid screening and assessment tool.

As mentioned at the beginning of this section there are two distinct recovery processes in carbonates, depending on whether or not fractures dominate the flow. If they do not, then viscous forces are significant for displacement through the porous matrix and local recovery is determined by the relative permeabilities. It is possible to perform a Buckley-Leverett analysis to compute, analytically, recovery for a homogeneous one-dimensional displacement from the relative permeabilities [7]. However, the likely local waterflood displacement efficiency can be estimated rapidly from direct inspection of the relative permeability curves. Imagine that the reservoir-condition oil and water viscosities are the same. Then, if the saturation near the production well is where the relative permeabilities cross, the subsurface ratio of oil to water production will be 1:1. Wells are abandoned when the cost of recycling and processing the produced water exceeds the economic benefit of the oil produced: this is normally when the oil:water ratio is between 1:2 and 1:10. On the other hand, the oil viscosity is typically greater than that of water, and the flow rate is determined by the ratio of relative permeability to viscosity. Hence, in most cases, production ceases close to where the relative permeabilities cross – between the producer, where water has displaced oil, the saturations will be higher, but this very simple trick allows a quick comparative study of recovery trends. Fig. 10 indicates that waterflooding is quite favourable in the less well connected carbonate samples – Estaillades and Ketton. Most of the moveable pore volume is displaced, and the residual saturation is low. The reason for this is that the poorly connected water phase holds back water advance, allowing the efficient displacement of oil. For the better connected sample, Mount Gambier, and for the experimental sample, the water relative permeability is higher, since the water is better connected and rapidly finds a pathway of large pores through the system. This allows water to bypass oil at the pore scale, leading to less favourable waterflood recovery.

Now consider a reservoir where flow is dominated by fractures. In this case the fractures effectively short-circuit the flow field and it is not possible to impose a substantial viscous pressure drop across the matrix. Recovery is mediated by capillary and gravitational forces. Imagine that water quickly invades the fractures surrounding a region of matrix (a so-called matrix block, although it does not have to be exactly, or even remotely, cuboidal in shape). Then recovery will occur by spontaneous imbibition – that is recovery will occur until the capillary pressure is zero. In our examples – see Fig. 9 – this means that only around 25% of the moveable pore volume is recovered. Furthermore, the rate of recovery is limited by the rate at which water can advance into the pore space – that is the relative permeability in the low water saturation range where the capillary pressure is positive. In this case now the more favourable system is the Mount Gambier – the water relative permeability is higher, indicating a more rapid displacement, while the degree of spontaneous imbibitions is larger, since the well-connected pore space allows all the water-wet regions of the rock to be accessed easily; in contrast the poorly connected Ketton and Estaillades has a lower water relative permeability and not all the water-wet regions of the pore space are interconnected, leading to less displacement at a positive capillary pressure.

Gravitational forces can also play an important role in the displacement. If water floods a vertical fracture and if oil – as is likely – is preferentially produced from the top of the matrix, then the weight of water in the fracture acts as a driving force. If we assume that the capillary pressure in the fractures is very small and is equal to zero at the top of a matrix block, then the capillary pressure at the base is $\Delta\rho gh$, where $\Delta\rho$ is the density difference between water and oil and h is the effective height of the matrix block. The capillary pressure is negative: the water has a higher pressure than oil. This allows forced displacement to a lower oil saturation. Taking typical values: $g = 9.81\ \mathrm{ms}^{-2}$; $\Delta\rho = 300\ \mathrm{kg\,m}^{-3}$ and, say, $h = 2$ m, then the negative capillary pressure that can be reached is around -6 kPa. Reading off the graph, Fig. 9(a), we can see that this driving force displaces a further 15% of the oil for the lowest permeability sample, Estaillades. Even if we consider lower permeability rocks (the capillary pressure approximately increases as $1/K^{1/2}$, where K is the permeability; see, for instance [140] where this scaling is applied to field-scale modelling), there is likely to be significant displacement with this driving force and demonstrates how both capillary and gravitational forces mediate recovery in field settings.

Gravity also determines the initial water saturation before waterflooding. As is apparent from Fig. 9, for the lowest permeability sample, Estaillades (which is still high permeability compared to most reservoir rocks) an effective matrix block height of around

10 m would be required to displace all the oil to close to residual saturation. There is a corollary to this: it also indicates that the initial saturation determined by capillary-gravity equilibrium (based, typically on the primary drainage capillary pressure) has a transition zone – with varying saturation above the irreducible value – of height around 10–100 m for rocks with permeabilities between 1mD and 100mD (using the $1/K^{1/2}$ scaling mentioned above). The initial water saturation affects both the wettability (at high saturation less of the rock is contacted directly by oil and, as the imposed capillary pressure is lower, the wettability alteration is likely to be less strong) and the starting point for waterflooding. There is often a wettability trend from water-wet near the oil–water contact, through mixed-wet in most of the reservoir with more oil-wet conditions at the crest. Usually, coreflood measurements are made from samples near the top of the reservoir: this could suggest oil-wet conditions and unfavourable waterflood recovery, when the reality is a much more efficient displacement in most of the reservoir column. Pore-scale modelling, allowing the prediction of relative permeabilities as a consistent function of initial water saturation, has enormous potential to improve the characterisation of such reservoirs [140].

This rather simple analysis already leads to some interesting and surprising conclusions. For the same wettability, in a reservoir where flow is not fracture dominated, local waterflood recovery is higher in the lower-permeability less well-connected sample, since the low water relative permeability holds back the water advance. On the other hand, if the reservoir is extensively fractured, the better-connected sample gives faster and better recovery, since a greater degree of spontaneous imbibition is allowed. This is a clear indication that both the nature of the reservoir – fractured or unfractured – and the multiphase flow properties are both crucial for any reasonable assessment of recovery. With pore-scale modelling potentially offering rapid predictions on hundreds of datasets with sensitivities on many different samples, the richness of the potential analysis goes far beyond current reservoir engineering approaches. However, there are also obvious difficulties: we did not provide predictions based on an image of the reservoir sample, since the typical pore sizes were below the resolution of the scanner we used, while in two of the samples ignoring micro-porosity is likely to have affected our predicted properties.

7. Discussion, conclusions and future challenges

This paper has presented three pore-scale imaging and modelling studies pertinent to different fields of application: contaminant transport, carbon dioxide storage in aquifers, and improved oil recovery. We have not attempted to review the whole range of properties that can currently be predicted using pore-scale modelling tools, but have simply highlighted some exemplar uses.

Direct simulation on pore-space images is now the modelling approach of choice for single-phase flow and transport, since the complexity of the pore-space geometry is preserved. We presented simulations of solute transport in three rock types: a sand pack, sandstone and carbonate. We demonstrated that in the heterogeneous carbonate studied, initially the peak of the plume was virtually immobile with a highly elongated leading edge; particles have to diffuse out of stagnant regions before they were able to move appreciably in the flow direction. The behaviour can be interpreted in the context of CTRW with a power-law distribution of travel times. This explains the highly anomalous behaviour that cannot be described by traditional models based on the advection–dispersion equation. At late time – assuming that the sample is macroscopically homogeneous over lengths of around 1 m – particles have sampled the entire flow field and a so-called asymptotic limit is reached where there is a well-defined dispersion coefficient. The dispersion coefficient increases with porous medium heterogeneity and there is a power-law relationship between the dispersion coefficient and Peclet number with an exponent related to the power-law distribution of travel times. The behaviour of the carbonate is qualitatively dissimilar to that of the other porous media studied, that show a less dispersed solute profile.

We imaged multiphase fluid distributions in a high-permeability sandstone to demonstrate that capillary trapping can locally sequester CO_2 occupying 25% of the pore space. The experiment used a novel high-pressure high-temperature flow cell with a carbon fibre sleeve to contain the rock and fluids. The work has important implications for carbon capture and storage, suggesting that CO_2 can be effectively trapped if displaced by water. The work is an important first step towards effective storage design: at the field scale the overall efficiency of storage will depend on the fraction of the reservoir volume contacted by CO_2 and then swept by water, while further tests are required to determine the amount of trapping for a representative range of temperatures and pressures, and for realistic reservoir samples, with more complex mineralogy, including carbonates.

For multiphase flow, network modelling still offers the quickest and most proven approach to predicting relative permeability and capillary pressure. We demonstrated a workflow involving imaging, network extraction, assignment of contact angle and simulation of displacement on three carbonates. We compared the computed properties with those measured on a reservoir sample. We discussed the implications of the results for field-scale recovery, distinguishing between recovery by waterflooding and by capillary imbibition.

While these – and many other – applications of pore-scale modelling are exceptionally promising, there are still many unresolved issues for future research. These are discussed below.

7.1. The challenge of scale

A problem that has been alluded to throughout this paper is how to model the enormous range of scales encountered in porous media, from the smallest pore spaces to the field scale. Based on our desire to reproduce laboratory experiments, modelling is presently somewhat artificially divided between pore-to-core prediction, and then upscaling for use in field-scale simulation. However, since natural systems are heterogeneous on all length scales, there is no obvious reason why this approach is anything other than a convenience constrained by our use of traditional reservoir simulators.

There is a need to develop an integrated suite of tools that find averaged properties at different scales and which can be properly incorporated into simulations of relevant flow and transport processes at larger scales. A possible approach is illustrated schematically in Fig. 11 that has been implemented for single-phase transport of a non-sorbing and non-reacting tracer [141]. The suite of modelling techniques described in this paper could be used for the pore-to-core characterisation of transport. In the context of single-phase flow, a CTRW approach, where the probability of transport across a domain in a given time is computed, shows some promise [141]. Conceptually, transport is considered as a series of hops between sites, using a generalised network model representation of the porous medium, where the hops can be at any spatial scale and are governed by a transit-time probability distribution derived from simulation at a smaller scale, faithfully representing the effects of heterogeneity. This probability can then be input into a simulation at the next larger scale – from cm to m – capturing heterogeneity that is not apparent in core samples. A new transit-time probability is computed and this can be used in a field-scale simulation. Generalising this approach to multiphase flow and more complex transport processes is a rich topic for

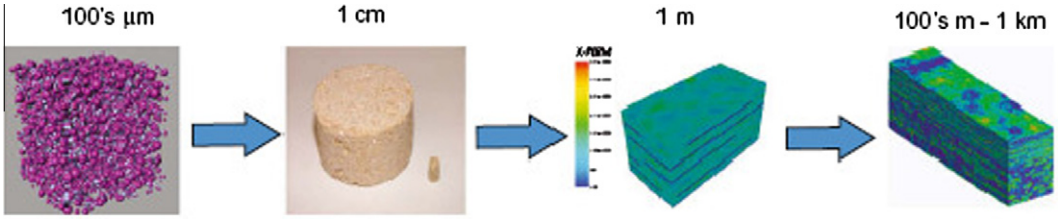

Fig. 11. A schematic of a potential upscaling method for flow and transport in porous media, integrating simulation approaches and data at different scales. At the pore-to-core scales a combination of direct simulation and network modelling – the focus of this paper – is making progress towards predictive capabilities. The upscaled characterisation of the flow can then be benchmarked and verified against core-scale measurements. These properties are than input into a simulation of transport at the metre scale – the scale of a typical field-scale simulation grid block. Again upscaled properties are used for the final step – reservoir simulation of the macroscopic process of interest. Figure adopted from [141].

future work. In addition, the simulations need to embrace and match data measured in different ways probing different scales and account for uncertainty in the fine details of the description of the porous medium.

Even if we consider the work presented in this paper, where our models have represented tiny pieces of rock a few mm across, and we have ignored upscaling, the challenge is enormous. In our dispersion work the images were 300^3, with the largest possible simulations using a workstation with 96 GB memory being 600^3, or, accounting for porosity, around 40 million void cells. With massively parallel computers, or the use of GPUs, larger simulations are possible, but the computation of even just the flow field on 1000^3 images is still not routine.

For multiphase flow, the problems of scale place a severe restriction on system size and simulation methodology. Consider, for instance, carbonate samples whose principal pore space could be imaged at a resolution of a few microns; in many cases there is significant connected porosity with pore sizes down to around 0.1 μm. In any event, to compute flow accurately, accounting for multiple phases in a single pore, and especially layers, a resolution of at least 0.1 μm is necessary. To be representative, a minimum overall size of the sample should be in the range of around 5 mm to capture pore-scale heterogeneity and may be considerably larger for samples with vugs and other core-scale heterogeneity. So the simulation size, based on a direct simulation is $50{,}000^3$ or more; this corresponds to a minimum of 10^{13} void voxels: ten trillion grid cells. While computing power is increasing rapidly, this is a frankly unrealistic system size now or in the future, and it is absurdly over-done – is it really necessary to have this much information to predict a relative permeability curve? Network modelling extracts a disordered lattice that preserves the main connectivity of the pore space without having to specify every small crack and cranny in the rock. By solving for flow in idealised elements, infinite resolution is achieved and it is feasible to make predictions of multiphase flow properties capturing the pore space geometry and the details of the flow physics. Rather than a competition between simulation methods, a more complimentary approach is needed, where direct simulation is used to elucidate displacement mechanisms and compute threshold capillary pressures on representative pores, or small groups of pores, for use in improved network models that then handle core-scale simulations of displacement.

In view of the lack of resolution in most simulations, and the considerable simplification of geometry made in network models, it is perhaps surprising that we obtain reasonable predictions of single and multiphase properties. To simplify the task we need to identify the key features that need to be captured and to neglect unnecessary details. To compute the flow field, it is necessary that the principal connected pore space is modelled; in many systems, the very small pores, below the image resolution, may make little contribution to the overall behaviour. In multiphase flow, the challenge is to account for the connectivity of two (or three) phases simultaneously. This again is possible if the main flow pathways are captured, together with a representation of the correct physics – such as layer drainage – within each pore and throat.

7.2. Characterisation and synthesis

Coupled to the problem of multiscale modelling, is the ability to characterise rock properties at the pore scale. Our focus here has been simply on distinguishing grain from pore over an appropriate range of length scales. However, to understand multiphase flow processes, this is not sufficient. The mineralogy will affect local contact angle and reaction: this can sometimes be inferred from images, but the consequences for transport are difficult to predict. One major uncertainty in multiphase flow prediction is the assignment of contact angle on a pore-by-pore basis which is, at present, performed on a somewhat *ad hoc* basis. Pore-scale wettability has been inferred from thin section images, obtained after waterflooding [142] while three-dimensional imaging can detect patterned wettability in simple porous media [143].

One idea is to integrate imaging and modelling together. For instance, very good images could be used to determine likely contact angles for samples of interest by estimating the angle of contact of the fluid interface with the solid. In addition, multiphase images could be used as the starting point for relative permeability prediction: rather than compute displacement numerically, the fluid configuration is provided by the images and flow is computed through each of the phases to find relative permeability [24]. Furthermore imaging, combined with direct pore-space modelling, could be used to identify and characterise pore-scale displacement mechanisms that can then be incorporated into network models. For instance, the present model for pore filling as a function of the number of connected throats filled with displacing fluid is somewhat crude [2,7] and detailed analysis of the problem on representative pore shapes could help frame a more realistic model.

7.3. Data integration

To make good predictions of flow and transport at all scales – from the pore to the reservoir – requires the integration of modelling tools and data. We have models appropriate at different scales – direct pore-space modelling, network modelling and reservoir simulation – combined with data acquired at different scales – seismic, production data, well test, logs, corefloods and images. At present we can use data at one scale for a model at that scale but find it difficult to incorporate all our information, from both models and experiments, into one consistent representation of the reservoir. The sophistication of our current modelling and imaging tools offers considerable promise in our efforts to understand multiphase flow; indeed it is possible that the challenge of understanding this wealth of data will lead to fundamental

breakthroughs, leading to a new basic foundation for the subject that moves away from the current empiricism based largely on experiments performed 30–40 years ago.

7.4. Unconventional resources

All the applications mentioned here have been conventional, in the sense that single and multiphase flow and transport was modelled in sandstones and carbonates where the fundamental governing equations – the Naver Stokes equation, Fick's law and the Young–Laplace equation – are valid. Unconventional hydrocarbon resources pose a new challenge for porous media research. Here oil and gas is contained in exceptionally low permeability shales with pore spaces in the source material – kerogen – just a few nm across in many cases. The physics of transport is a combination of molecular phenomena – sorption and diffusion – coupled to averaged, possibly Darcy-like flow in permeable fractures. A thorough, quantitative and predictive understanding of these systems is even more challenging than the examples mentioned previously and will require the coupling of simulations involving distinctly different physics at different scales.

Acknowledgements

The authors thank the sponsors of this research: Qatar Petroleum, Shell and the Qatar Science and Technology Park under the Qatar Carbonates and Carbon Storage Research Centre (QCCSRC); the Imperial College Consortium on Pore-Scale Modelling; and Shell through the Shell-Imperial Grand Challenge on Clean Fossil Fuels.

References

[1] Blunt MJ, Jackson MD, Piri M, Valvatne PH. Detailed physics, predictive capabilities and macroscopic consequences for pore-network models of multiphase flow. Adv Water Resour 2002;25:1069–89.
[2] Bakke S, Øren P-E. 3-D pore-scale modelling of sandstones and flow simulations in the pore networks. SPE J 1997;2:136–49.
[3] Øren P-E, Bakke S, Arntzen OJ. Extending predictive capabilities to network models. SPE J 1998;3:324–36.
[4] Øren P-E, Bakke S. Process based reconstruction of sandstones and prediction of transport properties. Transport Porous Med 2002;46(2–3):311–43.
[5] Øren P-E, Bakke S. Reconstruction of Berea sandstone and pore-scale modelling of wettability effects. J Petrol Sci Eng 2003;39:177–99.
[6] Patzek TW. Verification of a complete pore network simulator of drainage and imbibition. SPE J 2001;6:144–56.
[7] Valvatne PH, Blunt MJ. Predictive pore-scale modeling of two-phase flow in mixed wet media. Water Resour Res 2004;40:W07406. http://dx.doi.org/10.1029/2003WR002627.
[8] Piri M, Blunt MJ. Three-dimensional mixed-wet random pore-scale network modeling of two- and three-phase flow in porous media. I. Model description. Phys Rev E 2005;71:026301.
[9] Piri M, Blunt MJ. Three-dimensional mixed-wet random pore-scale network modeling of two- and three-phase flow in porous media. II. Results. Phys Rev E 2005;71:026302.
[10] Arns JY, Sheppard AP, Arns CH, Knackstedt MA, Yelkhovsky A, Pinczewski WV. Pore-level validation of representative pore networks obtained from micro-CT images. In: Proceedings of the annual symposium of the society of core analysis, SCA2007-A26, Calgary, Canada; 2007.
[11] Keehm Y, Mukerji T, Nur A. Permeability prediction from thin sections: 3D reconstruction and lattice-Boltzmann flow simulation. Geophys Res Lett 2004;31(4):L04606. http://dx.doi.org/10.1029/2003GL018761.
[12] Wildenschild D, Vaz C, Rivers M, Rikard D, Christensen B. Using X-ray computed tomography in hydrology: systems, resolutions, and limitations. J Hydrol 2002;267:285–97.
[13] Knackstedt M, Jaime P, Butcher AR, Botha PWSK, Middleton J, Sok, R. Integrating reservoir characterization: 3D dynamic, petrophysical and geological description of reservoir facies. In: Proceedings of the SPE Asia Pacific oil and gas conference and exhibition, 18–20 October, 2010, Brisbane, Queensland, Australia, SPE 133981; 2010.
[14] Wildenschild D. X-ray imaging and analysis techniques for quantifying pore-scale structure and processes in subsurface porous medium systems. Adv Water Resour 2013;51:217–46.
[15] Petrovic AM, Siebert JE, Rieke RE. Soil bulk-density analysis in 3 dimensions by computed tomographic scanning. Soil Sci Soc Am J 1982;46:445–50.
[16] Vinegar HJ, Wellington SL. Tomographic imaging of three-phase flow experiments. Rev Sci Instrum 1987;58:96–107.
[17] Flannery BP, Deckman HW, Roberge WG, D'Amico KL. Three-dimensional X-ray microtomography. Science 1987;237:1439–44.
[18] Dunsmuir JH, Ferguson SR, D'Amico KL, Stokes JP. X-ray microtomography. A new tool for the characterization of porous media. In: Proceedings of the 1991 SPE annual technical conference and exhibition, October 1991, Dallas, SPE 22860; 1991.
[19] Spanne P, Thovert JF, Jacquin CJ, Lindquist WB, Jones KW, Adler PM. Synchrotron computed microtomography of porous-media – topology and transports. Phys Rev Lett 1994;73:2001–4.
[20] Coker DA, Torquato S, Dunsmuir JH. Morphology and physical properties of Fontainebleau sandstone via a tomographic analysis. J Geophys Res Solid Earth 1996;101:17497–506.
[21] Hazlett RD. Simulation of capillary-dominated displacements in microtomographic images of reservoir rocks. Transport Porous Med 1995;20(1–2):21–35.
[22] Ketcham RA, Carlson WD. Acquisition, optimization and interpretation of X-ray computed tomographic imagery: applications to the geosciences. Comput Geosci 2001;27:381–400.
[23] Arns CH, Bauget F, Limaye A, Sakellariou A, Senden TJ, Sheppard AP, et al. Pore-scale characterization of carbonates using X-ray microtomography. SPE J 2005;10(4):475–84.
[24] Turner ML, Knufing L, Arns CH. Three-dimensional imaging of multiphase flow in porous media. Physica A 2004;339(1–2):166–72.
[25] Münch B, Trtik P, Marone F, Stampanoni M. Stripe and ring artifact removal with combined wavelet–fourier filtering. Opt Express 2009;17(10):8567–91.
[26] Hossain Z, Moller T. Edge aware anisotropic diffusion for 3D scalar data. IEEE Trans Vis Comput Graph 2010;16(6):1376–85.
[27] Otsu N. IEEE Trans Syst Man Cybernet 1979;9:62–6.
[28] Iglauer S, Paluszny A, Pentland CH, Blunt MJ. Residual CO_2 imaged with X-ray micro-tomography. Geophys Res Lett 2001;38:L21403.
[29] Lemmens HJ, Butcher AR, Botha PWSK. FIB/SEM and automated mineralogy for core and cuttings analysis. In: Proceedings of the SPE Russian oil and gas conference and exhibition, 26–28 October, 2010, Moscow, Russia, SPE 136327; 2010.
[30] Tomutsa L, Silin D. Analysis of chalk petrophysical properties by means of submicron-scale pore imaging and modeling. SPE Reservoir Eval Eng 2007;10(3):285–93.
[31] Fredrich JT. 3D imaging of porous media using laser scanning confocal microscopy with application to microscale transport processes. Phys Chem Earth A. Solid Earth Geodesy 1999;24(7):551–61.
[32] Strebelle S. Conditional simulation of complex geological structures using multiple-point statistics. Math Geol 2002;34:1–21.
[33] Okabe H, Blunt MJ. Prediction of permeability for porous media reconstructed using multiple-point statistics. Phys Rev E 2004;70:066135.
[34] Jiang Z, Wu K, Couples G, Van Dijke MIJ, Sorbie KS, Ma J. Efficient extraction of networks from three-dimensional porous media. Water Resour Res 2007;43(12):W12S02.
[35] Wu K, Van Dijke MIJ, Couples GD, Sorbie KS, Ma J. 3D stochastic modelling of heterogeneous porous media – Applications to reservoir rocks. Transport Porous Med 2006;65(3):443–67.
[36] Sok RM, Varslot T, Ghous A. Pore scale characterization of carbonates at multiple scales: integration of Micro-CT, BSEM, and FIBSEM. Petrophysics 2010;51(6):379–87.
[37] Chen S, Doolen GD. Lattice Boltzmann method for fluid flows. Annu Rev Fluid Mech 1998;30:329–64.
[38] Kang Q, Lichtner PC, Zhang D. Lattice Boltzmann pore-scale model for multicomponent reactive transport in porous media. J Geophys Res 2006;111:B05203.
[39] Manwart C, Aaltosalmi U, Koponen A, Hilfer R, Timonen J. Lattice-Boltzmann and finite-difference simulations for the permeability for three-dimensional porous media. Phys Rev E 2002;66:16702–13.
[40] Porter ML, Schaap MG, Wildenschild D. Lattice-Boltzmann simulations of the capillary pressure–saturation–interfacial area relationship for porous media. Adv Water Resour 2009;32(11):1632–40.
[41] Schaap MG, Porter ML, Christensen BSB, Wildenshild D. Comparison of pressure-saturation characteristics derived from computed tomography and lattice Boltzmann simulations. Water Resour Res 2007;43:W12S06.
[42] Pan C, Hilpert M, Miller CT. Lattice-Boltzmann simulation of two-phase flow in porous media. Water Resour Res 2004;40:W01501.
[43] Hao L, Cheng P. Pore-scale simulations on relative permeabilities of porous media by lattice Boltzmann method. Int J Heat Mass Transfer 2010;53(9–10):1908–13.
[44] Boek ES, Venturoli M. Lattice-Boltzmann studies of fluid flow in porous media with realistic rock geometries. Comput Math Appl 2010;59(7):2305–14.
[45] Ramstad T, Idowu N, Nardi C, Øren P-E, Relative permeability calculations from two-phase flow simulations directly on digital images of porous rocks. Transport Porous Med 2011; doi:http://dx.doi.org/10.1007/s11242-011-9877-8.
[46] Tartakovsky AM, Ferris KF, Meakin P. Lagrangian particle model for multiphase flows. Comput Phys Commun 2009;180(10):1874–81.
[47] Ovaysi S, Piri M. Direct pore-level modeling of incompressible fluid flow in porous media. J Comput Phys 2010;229:7456–76.
[48] Sussman M, Smereka P, Osher S. A level set approach for computing solutions to incompressible two-phase flow. J Comput Phys 1994;114(1):146–59.

[49] Prodanovic M, Bryant SL, Karpyn ZT. Investigating matrix/fracture transfer via a level set method for drainage and imbibition. SPE J 2010;15(1):125–36.
[50] Renardy M, Renardy Y, Li J. Numerical simulation of moving contact line problems using a volume-of-fluid method. J Comput Phys 2001;263:243–63.
[51] Renardy Y, Renardy M. A parabolic reconstruction of surface tension for the volume-of-fluid method. J Comput Phys 2002;421:400–21.
[52] Raeini AQ, Blunt MJ, Bijeljic B. Modelling two-phase flow in porous media at the pore scale using the volume-of-fluid method. J Comput Phys; in press.
[53] Demianov A, Dinariev O, Evseev N. Density functional modelling in multiphase compositional hydrodynamics. Can J Chem Eng 2011;89:207–26.
[54] Meakin P, Tartakovsky AM. Modeling and simulation of pore-scale multiphase fluid flow and reactive transport in fractured and porous media. Rev Geophys 2009;47:RG3002.
[55] Fatt I. The network model of porous media I. Capillary pressure characteristics. Trans AIME 1956;207:144–59.
[56] Yiotis AG, Tsimpanogiannis IN, Stubos AK, Yortsos YC. Pore-network study of the characteristic periods in the drying of porous materials. J Colloid Interface Sci 2006;297(2):738–48.
[57] Lopez X, Valvatne PH, Blunt MJ. Predictive network modeling of single-phase non-Newtonian flow in porous media. J Colloid Interface Sci 2003;264(1):256–65.
[58] Balhoff MT, Wheeler MF. A predictive pore-scale model for non-Darcy flow in porous media. SPE J 2009;14(3):579–87.
[59] Ryazanov AV, van Dijke MIJ, Sorbie KS. Two-phase pore-network modelling: existence of oil layers during water invasion. Transport Porous Med 2009;80:79–99.
[60] Idowu NA, Blunt MJ. Pore-scale modelling of rate effects in waterflooding. Transport Porous Med 2010;83:151–69.
[61] Lovoll G, Meheust Y, Maloy KJ, Aker E, Schmittbuhl J. Competition of gravity, capillary and viscous forces during drainage in a two-dimensional porous medium, a pore scale study. Energy 2005;30(6):861–72.
[62] Nguyen VH, Sheppard AP, Knackstedt MA, Pinczewski WV. The effect of displacement rate on imbibitions relative permeability and residual saturation. J Petrol Sci Eng 2006;52(1–4):54–70.
[63] Tørå G, Øren P-E, Hansen A. Dynamic network model for two-phase flow in porous media. Transport Porous Med 2012;92:145–64.
[64] Lindquist WB, Venkatarangan A. Investigating 3D geometry of porous media from high resolution images. Phys Chem Earth A. Solid Earth Geod 1999;24:593–9.
[65] Lindquist WB, Venkatarangan A, Dunsmuir J, Wong TF. Pore and throat size distributions measured from synchrotron X-ray tomographic images of Fontainebleau sandstones. J Geophys Res Solid Earth 2000;105: 21509–27.
[66] Silin D, Patzek T. Pore space morphology analysis using maximal inscribed spheres. Physica A 2006;371:336–60.
[67] Dong H, Blunt MJ. Pore-network extraction from micro-computerized-tomography images. Phys Rev E 2009;80:036307. http://dx.doi.org/10.1103/PhysRevE.80.036307.
[68] Patankar SV, Spalding DB. A calculation procedure for heat, mass and momentum transfer in three-dimensional parabolic flows. Int J Heat Mass Transfer 1972;15:1787–806.
[69] Stüben K. A review of algebraic multigrid. J Comput Appl Math 2001;128:281–309.
[70] Mostaghimi P, Bijeljic B, Blunt MJ. Simulation of flow and dispersion on pore-space images. In: Proceedings of the SPE annual technical conference and exhibition, Florence, Italy, SPE 135261; 2010.
[71] OpenFOAM. The open source CFD toolbox. <http://www.openfoam.com>; 2011.
[72] de Arcangelis L, Koplik J, Redner S, Wilkinson D. Hydrodynamic dispersion in network models of porous media. Phys Rev Lett 1986;57:996–9.
[73] Sahimi M, Hughes BD, Scriven LE, Davis TH. Dispersion in flow through porous media – I. One-phase flow. Chem Eng Sci 1986;41:2103–22.
[74] Sorbie KS, Clifford PJ. The inclusion of molecular diffusion effects in the network modelling of hydrodynamic dispersion in porous media. Chem Eng Sci 1991;46:2525–42.
[75] Manz B, Gladden LF, Warren PB. Flow and dispersion in porous media: lattice Boltzmann and NMR studies. AIChE J 1999;45:1845–54.
[76] Maier RS, Kroll DM, Bernard RS, Howington SE, Peters JF, Davis HT. Pore-scale simulation of dispersion. Phys Fluids 2000;12:2065–80.
[77] Bruderer C, Bernabé Y. Network modeling of dispersion: transition from Taylor dispersion in homogeneous networks to mechanical dispersion in very heterogeneous ones. Water Resour Res 2001;37:897–908.
[78] Acharya RC, Van Dijke MIJ, Sorbie KS, Van der See SEATM, Leijnse A. Quantification of longitudinal dispersion by upscaling Brownian motion of tracer displacement in a 3D pore-scale network model. Adv Water Resour 2007;30(2):199–213.
[79] Acharya RC, Van der Zee S, Leijnse A. Approaches for modeling longitudinal dispersion in pore-networks. Adv Water Resour 2007;30:261–72.
[80] Zhang X, Lv M. Persistence of anomalous dispersion in uniform porous media demonstrated by pore-scale simulations. Water Resour Res 2007;43:W07437.
[81] Cardenas MB. Direct simulation of pore level Fickian dispersion scale for transport through dense cubic packed spheres with vortices. Geochem Geophys Geosyst 2009;10:Q12014.
[82] Zhao W, Picard G, Leu G, Singer PM. Characterization of single-phase flow through carbonate rocks: quantitative comparison of NMR flow propagator measurements with a realistic pore network model. Transport Porous Med 2010;81:305–15.
[83] Bijeljic B, Muggeridge AH, Blunt MJ. Pore-scale modeling of longitudinal dispersion. Water Resour Res 2004;40:W11501.
[84] Bijeljic B, Blunt MJ. Pore-scale modeling and continuous time random walk analysis of dispersion in porous media. Water Resour Res 2006;42(1):W01202.
[85] Jha RK, Bryant SL, Lake LW. Effect of diffusion on dispersion. SPE J 2011;16(1):65–77.
[86] Ovaysi S, Piri M. Pore-scale modeling of dispersion in disordered porous media. J Contam Hydrol 2011;124:68–81.
[87] Bijeljic B, Mostaghimi P, Blunt MJ. The signature of non-Fickian transport in highly heterogeneous media. Phys Rev Lett 2011;107:204502.
[88] Dentz M, Cortis A, Scher H, Berkowitz B. Time behavior of solute transport in heterogeneous media: transition from anomalous to normal transport. Adv Water Resour 2004;27:155–73.
[89] Berkowitz B, Cortis A, Dentz M, Scher H. Modelling non-Fickian transport in geological formations as a continuous time random walk. Rev Geophys 2006;44:RG2003.
[90] Pollock DW. Semianalytical computation of path lines for finite-difference models. Ground Water 1988;26:743–50.
[91] Scheven UM, Verganelakis D, Harris R, Johns ML, Gladden LF. Quantitative nuclear magnetic resonance measurements of preasymptotic dispersion in flow through porous media. Phys Fluids 2005;17:117107.
[92] Mitchell J, Graf von der Schulenburg DA, Holland DJ, Fordham EJ, Johns ML, Gladden LF. Determining NMR flow propagator moments in porous rocks without the influence of relaxation. J. Magn. Reson. 2008;193:218–25.
[93] Harris RJ, Sederman AJ, Mantle MD, Crawshaw J, Johns ML. A comparison of experimental and simulated propagators in porous media using confocal laser scanning microscopy, lattice Boltzmann hydrodynamic simulations and nuclear magnetic resonance. Magn. Reson. Imaging 2005;23:355–7.
[94] Maier RS, Schure MR, Gage JP, Seymour JD. Sensitivity of pore-scale dispersion to the construction of random bead packs. Water Resour Res 2008;44:W06S03.
[95] Sahimi M. Flow and transport in porous media and fractured rock. Wiley-VCH Verlag GmbH; 1995.
[96] Pfannkuch HO. Contribution à l'étude des déplacements de fluides miscibles dans un milieu poreux. Revue-Institut Français du Pétrole 1963;18:215–70.
[97] Ding A, Candela D. Probing nonlocal tracer dispersion in flows through random porous media. Phys Rev E 1996;54:656–60.
[98] Seymour JD, Callaghan PT. Generalized approach to NMR analysis of flow and dispersion in porous media. AIChE J 1997;43:2096–111.
[99] Kandhai D, Hlushkou D, Hoekstra AG, Sloot PMA, Van As H, Tallarek U. Influence of stagnant zones on transient and asymptotic dispersion in macroscopically homogeneous porous media. Phys Rev Lett 2002;88:234501.
[100] Khrapitchev AA, Callaghan PT. Reversible and irreversible dispersion in a porous medium. Phys Fluids 2003;15:2561–649.
[101] Drazer G, Chertcoff R, Bruno L, Rosen M, Hulin JP. Tracer dispersion in packings of porous activated carbon grains. Chem Eng Sci 1999;54:4137–44.
[102] Stöhr M. Analysis of flow and transport in refractive index matched porous media. PhD. Thesis. Germany: University of Heidelberg; 2003.
[103] Aggelopoulos CA, Tsakiroglou CD. The longitudinal dispersion coefficient of soils as related to the variability of local permeability. Water Air Soil Pollut 2007;185:223–37.
[104] Theodoropoulou MA. Dispersion of dissolved contaminants in groundwater: from visualization experiments to macroscopic simulation. Water Air Soil Pollut 2007;181:235–45.
[105] Adams EE, Gelhar LW. Field study of dispersion in a heterogeneous aquifer: 2. Spatial moments analysis. Water Resour Res 1992;28:3293–307.
[106] Riaz A, Hesse M, Tchelepi HA, Orr FM. Onset of convection in a gravitationally unstable diffusive boundary layer in porous media. J Fluid Mech 2006;548:87–111.
[107] Hidalgo JJ, Carrera J. Effect of dispersion on the onset of convection during CO_2 sequestration. J Fluid Mech 2009;640:441.
[108] Ennis-King J, Paterson L. Role of convective mixing in the long-term storage of carbon dioxide in deep saline formations. SPE J 2005;10(3):349–56.
[109] Pruess K, Garcia J. Multiphase flow dynamics during CO_2 disposal into saline aquifers. Environ Geol 2002;42(2–3):282–95.
[110] Hesse MA, Orr FM, Tchelepi HA. Gravity currents with residual trapping. J Fluid Mech 2008;611:35–60.
[111] Intergovernmental Panel on Climate Change (IPCC). IPCC special report on carbon dioxide capture and storage. In: Prepared by working group iii of the intergovernmental panel on climate change. Cambridge University Press; 2005.
[112] Xu TF, Apps JA, Pruess K. Reactive geochemical transport simulation to study mineral trapping for CO_2 disposal in deep saline arenaceous aquifers. J Geophys Res 2003;108:2071–84.
[113] Kumar A, Ozah R, Noh M, Pope GA, Bryant S, Sepehrnoori K, Lake LW. Reservoir simulation of CO_2 storage in deep saline aquifers. SPE J 2005;10(3):336–48.
[114] Juanes R, Spiteri EJ, Orr FM, Blunt MJ. Impact of relative permeability hysteresis on geological CO_2 storage. Water Resour Res 2006;42:W12418.
[115] Suekane T, Nobuso T, Hirai S, Kiyota M. Geological storage of carbon dioxide by residual gas and solubility trapping. Int J Greenhouse Gas Control 2008;2(1):58–64.
[116] Qi R, LaForce TC, Blunt MJ. Design of carbon dioxide storage in aquifers. Int J Greenhouse Gas Control 2009;3:195–205.

[117] Roof JG. Snap-off of oil droplets in water-wet pores. SPE J 1970;10:85–90.
[118] Lenormand R, Zarcone C, Sarr A. Mechanisms of the displacement of one fluid by another in a network of capillary ducts. J Fluid Mech 1983;135:337–53.
[119] Blunt MJ, Scher H. Pore level modeling of wetting. Phys Rev E 1995;52:6387–403.
[120] Pentland CH, El-Maghraby R, Iglauer S, Blunt MJ. Measurements of the capillary trapping of super-critical carbon dioxide in Berea sandstone. Geophys Res Lett 2011;38:L06401.
[121] Chalbaud C, Robin M, Lombard J-M, Martin F, Egermann P, Bertin H. Interfacial tension measurements and wettability evaluation for geological CO_2 storage. Adv Water Resour 2009;32(1):98–109.
[122] Plug WJ, Bruining J. Capillary pressure for the sand–CO_2–water system under various pressure conditions. Application to CO_2 sequestration. Adv Water Resour 2007;30(11):2339–53.
[123] Chiquet P, Broseta D, Thibeau S. Wettability alteration of caprock minerals by carbon dioxide. Geofluids 2007;7(2):112–22.
[124] Prodanović M, Lindquist WB, Seright RS. 3D image-based characterization of fluid displacement in a Berea core. Adv Water Resour 2007;30:214–26.
[125] Kumar M, Senden TJ, Sheppard AP. Visualizing and quantifying the residual phase distribution in core material. Petrophysics 2010;51(5):323–32.
[126] Karpyn Z, Piri M, Singh G. Experimental investigation of trapped oil clusters in a water-wet bead pack using X-ray microtomography. Water Resour Res 2010;46:W04510.
[127] Knackstedt M, Senden T, Carnerup A, Fogden A. Improved characterization of EOR processes in 3D. Characterizing mineralogy, wettability and residual fluid phases at the pore scale. In: Proceedings of the SPE enhanced oil recovery conference, 19–21 July, 2011, Kuala Lumpur, Malaysia, SPE 145093.
[128] Iglauer S, Favretto S, Spinelli G, Schena G, Blunt MJ. X-ray tomography measurements of power-law cluster size distributions for the nonwetting phase in sandstones. Phys Rev E 2010;82(5):056315.
[129] Landry CJ, Karpyn ZT, Piri M. Pore-scale analysis of trapped immiscible fluid structures and fluid interfacial areas in oil-wet and water-wet bead packs. Geofluids 2011;11:209–27.
[130] Iglauer S, Fernø MA, Shearing P, Blunt MJ. Comparison of residual oil cluster size distribution, morphology and saturation in oil-wet and water-wet sandstone. J Colloid Interface Sci 2012;375:187–92.
[131] Silin D, Tomutsa L, Benson SM, Patzek TW. Microtomography and pore-scale modeling of two-phase fluid distribution. Transport Porous Med 2011;86:495–515.
[132] Hassler GL. US Patent 2345,935; 1944.
[133] Tschumperlé D, Deriche R. In: Proceedings of the IEEE computer society conference on computer vision and pattern recognition, vol. 1; 2003. p. 651–6.
[134] Ahlbrandt TS. Global resource estimates from total petroleum systems. In: 86 AAPG; 2005.
[135] Behbahani H, Blunt MJ. Analysis of imbibition in mixed-wet rocks using pore-scale modeling. SPE J 2005;10(4):466–74.
[136] Al-Kharusi AS, Blunt MJ. Multiphase flow predictions from carbonate pore space images using extracted network models. Water Resour Res 2008;44:W06S01.
[137] Zhao X, Blunt MJ, Yao J. Pore-scale modeling: effects of wettability on waterflood oil recovery. J Petrol Sci Eng 2010;71:169–78.
[138] Jiang Z, van Dijke MIJ, Wu K, Couples GD, Sorbie KS, Ma J. Stochastic pore network generation from 3D rock images. Transport Porous Med 2011. http://dx.doi.org/10.1007/s11242-011-9792-z.
[139] Al Sayari SS. The influence of wettability and carbon dioxide injection on hydrocarbon recovery. PhD Thesis. London: Imperial College; 2009.
[140] Jackson MD, Valvatne PH, Blunt MJ. Prediction of wettability variation and its impact on flow using pore- to reservoir-scale simulations. J Petrol Sci Eng 2003;39:231–46.
[141] Rhodes ME, Bijeljic B, Blunt MJ. Pore-to-field simulation of single-phase transport using continuous time random walks. Adv Water Resour 2008;31(2):1527–39.
[142] Fassi-Fihri O, Robin M, Rosenberg E. Wettability studies at the pore level. A new approach by the use of Cryo-Scanning Electron Microscopy. In: Proceedings of the 1991 SPE annual technical conference and exhibition, Dallas, SPE 22596; 1991.
[143] Kumar M, Fogden A. Patterned wettability of oil and water in porous media. Langmuir 2010;26(6):4036–47.